Path following for the PVTOL aircraft ⋆

Luca Consolini [a], Manfredi Maggiore [b], Christopher Nielsen [c], Mario Tosques [d]

[a] *Dipartimento di Ingegneria dell'Informazione, Parco Area delle Scienze 181/a, 43100 Parma, Italy.*

[b] *Electrical and Computer Engineering Department, University of Toronto, 10 King's College Road, Toronto, Ontario, M5S 3G4, Canada.*

[c] *Department of Electrical and Computer Engineering, University of Waterloo, 200 University Ave. W, Waterloo, Ontario, N2L 3G1, Canada.*

[d] *Dipartimento di Ingegneria Civile, Parco Area delle Scienze 181/a, 43100 Parma, Italy.*

Abstract

This article presents a solution to the path following problem for the planar vertical take-off and landing aircraft (PVTOL) which is applicable to a class of smooth Jordan curves. Our path following methodology enjoys the two properties of output invariance of the path (i.e., if the PVTOL's centre of mass is initialized on the path and its initial velocity is tangent to the path, then the PVTOL remains on the path at all future time) and boundedness of the roll dynamics. Further, our controller guarantees that, after a finite time, the time average of the roll angle is zero, and the PVTOL does not perform multiple revolutions about its longitudinal axis.

Key words: path following, planar vertical take-off and landing aircraft, set stabilization, controlled invariant submanifolds, path invariance, Hamiltonian dynamics, transverse feedback linearization, virtual holonomic constraints, Jordan curves.

1 Introduction

In this paper we investigate the model of a V/STOL aircraft in planar vertical take-off and landing (PVTOL) mode, introduced by Hauser, Sastry and Meyer in [10]

$$\begin{aligned}
\dot{x}_1 &= x_2 \\
\dot{x}_2 &= -u_1 \sin x_5 + \epsilon u_2 \cos x_5 \\
\dot{x}_3 &= x_4 \\
\dot{x}_4 &= -g + u_1 \cos x_5 + \epsilon u_2 \sin x_5 \\
\dot{x}_5 &= x_6 \\
\dot{x}_6 &= \mu u_2 \\
y &= h(x) = \operatorname{col}(x_1, x_3),
\end{aligned} \tag{1}$$

⋆ This paper was not presented at any IFAC meeting. Corresponding author M. Maggiore. Tel. +1 416-946-5095. Fax +1 416-978-0804.

Email addresses: lucac@ce.unipr.it (Luca Consolini), maggiore@control.utoronto.ca (Manfredi Maggiore), cnielsen@uwaterloo.ca (Christopher Nielsen), mario.tosques@unipr.it (Mario Tosques).

Published in *Automatica*, vol. 46, 2010, pp. 1284–1296

where (x_1, x_3) are the coordinates of the centre of mass of the aircraft in the vertical plane, x_5 is the roll angle, and (x_2, x_4, x_6) are the corresponding velocities. The constants ϵ and μ are positive, and g denotes the acceleration due to gravity. The state space of the PVTOL is $M = \mathbb{R}^4 \times (\mathbb{R} \bmod 2\pi) \times \mathbb{R}$. The output of the system is the position of the aircraft's centre of mass, (x_1, x_3). In various computations we will denote by f, g_1, and g_2 the drift and control vector fields in (1), so that $\dot{x} = f(x) + g_1(x)u_1 + g_2(x)u_2$.

The PVTOL control system (1) has become a benchmark for controller design used in unmanned aerial vehicle applications. The bulk of existing research can be partitioned into two main categories: set-point stabilization [20], [23], [24], [26], [27] and design of tracking or path following controllers [1], [4], [5], [12], [13], [15], [19]. This paper falls into the latter category and deals with the path following problem.

It is well-known that when the centre of mass (x_1, x_3) of the PVTOL is used as an output, the resulting zero dynamics are non-minimum phase, i.e., they are not asymptotically stable. This fact presents a challenge to controller design. In particular, if one is not careful in designing a tracking controller, the VTOL will begin to rotate about its longitudinal axis uncontrollably making several rotations as the vehicle executes the trajectory. In [14], [15] the authors overcome this problem by using the Huygens centre of oscillation as an alternative output yielding a fully feedback linearizable system; see also [23]. A nonlinear output regulation approach to tracking was studied in [13]. There, the authors make the vertical displacement x_3 track a sinusoidal signal in the presence of disturbances and unknown model parameters, while keeping the aircraft perfectly horizontal, and with no lateral movement. In this special case, the tracking problem is greatly simplified, as it is only during lateral movements that the coupling between lateral and vertical thrusts becomes problematic.

The fact that PVTOL has non-minimum phase zero dynamics associated with its centre of mass suggests that path following controllers may be more appropriate than tracking controllers. In a tracking control approach, the path to be followed is parameterized by time, and the parametrization becomes the reference signal. Tracking such a time parametrization is not always suitable for the PVTOL: moving along the path too quickly can lead to the undesirable rotations mentioned earlier. In contrast to tracking controllers, path following controllers do not rely on an a priori parameterization of the curve to be followed and have the potential to overcome the performance limitations inherent with tracking controllers.

In [1], the authors use non-causal system inversion to design a tracking controller and then convert it to a path following controller by means of a popular projection technique introduced in [9]. The authors demonstrate their ideas on a circular path. In [4], it is shown that there exists a constant κ such that for every C^2 closed curve $\gamma(t)$ with $\|\ddot{\gamma}\|_\infty \leq \kappa$, it is possible to find suitable initial conditions for the roll angle and velocity such that the centre of mass exactly tracks γ and the aircraft does not overturn. The authors show that any C^2 closed curve can be exactly tracked with bounded roll angle variation, provided the curve is reparameterized in such a way that the reference point moves sufficiently slowly along the curve. The same problem is investigated in [19]. There, the authors define a desired ("quasi-static") trajectory for the roll dynamics and formulate a nonlinear optimal control problem whose solution yields a feasible trajectory that approximates the quasi-static one and has bounded roll angle variations.

The three approaches reviewed above do not produce controllers in closed form, because they rely on iterative algorithms to compute feasible trajectories. In this paper, we design a closed-form path following controller driving the centre of mass of the PVTOL to a curve and making it traverse the curve in a desired direction. Our approach applies to a large class of smooth Jordan curves with a vertical axis of symmetry. The assumptions on the path geometry are described in detail in Section 2.

We take a nested set stabilization approach to solve the problem. We first stabilize a four-dimensional submanifold of the state space, $\Gamma_1^\star$, on which the centre of mass of the PVTOL is constrained to lie on the path. We further stabilize a two dimensional submanifold $\Gamma_2^\star \subset \Gamma_1^\star$ that corresponds to a "virtual constraint" specifying what should be the roll angle of the PVTOL at any given point on the path. The proposed solution to the path following problem is local in the sense that the controller is guaranteed to work for all initial conditions in a neighborhood of $\Gamma_2^\star$. In particular, the centre of mass of the PVTOL can be initialized in a neighborhood of the path.

With the proposed controller, the PVTOL enjoys the feature of *output invariance of the path*, by which we mean that if the PVTOL's centre of mass starts on the path with initial velocity tangent to it, then it will remain on the path for all future time. This is desirable because once the aircraft is on the path with the correct velocity vector, the path is followed exactly, which is essential to avoid collisions with the ground. Our design also guarantees boundedness of the roll dynamics of the PVTOL and that, after a finite time, the time average of the roll angle is zero, and the

PVTOL does not perform multiple revolutions about its longitudinal axis. A feature of our approach, as apposed to exact tracking approaches in the literature (including [4] and [19]), is that it doesn't require any upper bound on the speed with which the PVTOL traverses the path.

Interestingly, when the path to be followed is a circle, the problem of making the PVTOL travel around the circle while not performing full rotations about its longitudinal axis is equivalent to controlling the pendubot system and ensuring that the outer link does not make full rotations about its pivot point, while the inner link rotates. In [6], the authors use virtual constraints to design controllers that achieve two types of periodic motions of the outer link in the pendubot. The periodic motion of the outer link is determined by the choice of virtual constraint. Thus, our control approach is philosophically similar to that in [6], although the choice of virtual constraint and the analysis are entirely different.

Notation. If N is a positive real number, $[\cdot]_N : \mathbb{R} \to \mathbb{R} \bmod N$ is the function mapping real numbers to their value modulo N, so for instance $[7\pi/2]_{2\pi} = 3\pi/2$. Two points x and $x + N$ are mapped by $[\cdot]_N$ to the same point in $\mathbb{R} \bmod N$ in the same way that two points with angles θ and $\theta + 2\pi$ are identified on the unit circle. Therefore, the set $\mathbb{R} \bmod N$ can be given the geometric structure of a circle. In the following, we will consider a curve of length L, and will denote $S^1 := \mathbb{R} \bmod L$. Given vectors $x, y \in \mathbb{R}^n$, we will denote by $\langle x, y \rangle$ the Euclidean inner product and by $\|x\|$ the associated Euclidean norm. Given a set $A \subset \mathbb{R}^n$, and a point $x \in \mathbb{R}^n$, we let $\|x\|_A := \inf_{a \in A} \|x - a\|$. We let $\operatorname{col}(x_1, \ldots, x_k) = [x_1 \ \cdots \ x_k]^\top$. Given a function $\sigma : A \to B$, we let $\operatorname{Im}(\sigma)$ denote its image, i.e., $\operatorname{Im}(\sigma) = \{y \in B : y = \sigma(x), \text{ for some } x \in A\}$. If $f(x_1, \ldots, x_n)$ is a differentiable function, we denote by $\partial_{x_i} f$ its partial derivative with respect to x_i.

If M and N are two smooth manifolds and $F : M \to N$ is a map, we denote by dF_p the differential of F at $p \in M$. If M and N are open subsets of Euclidean spaces $\mathbb{R}^m$ and $\mathbb{R}^n$, respectively, then dF_p is the familiar derivative of F at p, whose matrix representation is the $n \times m$ Jacobian of F. In this case, we will not distinguish, notationally, between the map dF_p and its matrix representation. In particular, if $\lambda : \mathbb{R}^n \to \mathbb{R}$ is a real-valued function then, depending on the context, $d\lambda_x$ may represent the differential map $\mathbb{R}^n \to \mathbb{R}$ or the row vector $[\partial_{x_1}\lambda \ \cdots \ \partial_{x_n}\lambda]$. On the other hand, we will denote by $\nabla_x \lambda$ the column vector $d\lambda_x^\top$. Given a vector field f, the directional derivative of λ along f, denoted by $L_f\lambda$, is given by $L_f\lambda(x) = \langle d\lambda_x, f(x) \rangle$. If $\phi : \mathbb{D} \to M$ is a smooth map between manifolds, with either $\mathbb{D} = \mathbb{R}$ or $\mathbb{D} = \mathbb{R} \bmod N$, and $d/d\theta$ is the tangent vector to $\mathbb{D}$ at θ, we will denote by $\phi'(\theta) := d\phi_\theta(d/d\theta)$ the tangent vector at $\phi(\theta)$, which we identify with a vector in $\mathbb{R}^m$, where $m = \dim M$, so that the function $\theta \mapsto \phi'(\theta)$ maps $\mathbb{D} \to \mathbb{R}^m$. Then, the second derivative $\phi''(\theta)$ is also a function $\mathbb{D} \to \mathbb{R}^m$.

Organization of the paper. In Section 2 we present the class of curves, the path following problem, and we outline the steps we take to solve it. The steps are elaborated in detail in Section 3. The complete path following controller and the main stability result are presented in Section 4. In Section 5 we present various examples and discuss how to implement our controller in the two cases when curves are represented parametrically or in implicit form.

2 Path following problem

Consider a regular Jordan curve (i.e., a regular simple closed curve) $\mathcal{C}$ of length L in the y plane with smooth parameterization $\tilde{\sigma}(\cdot) : \mathbb{R} \to \mathbb{R}^2$, $\operatorname{Im}(\tilde{\sigma}) = \mathcal{C}$. Assume, without loss of generality, that $\tilde{\sigma}$ is a unit speed parameterization, i.e., $\|\tilde{\sigma}'(\cdot)\| \equiv 1$. With this assumption, the map $\tilde{\sigma}$ is L-periodic. Being a Jordan curve in $\mathbb{R}^2$, $\mathcal{C}$ can also be expressed in implicit form as

$$\mathcal{C} = \{y \in W : \gamma(y) = 0\},$$

where $\gamma : W \subset \mathbb{R}^2 \to \mathbb{R}$ is a smooth function such that $d\gamma_y \neq 0$ on W, and W is an open set containing $\mathcal{C}$. In Section 5.2 we illustrate one way to determine γ from a parametrization of $\mathcal{C}$. Without loss of generality, we will assume that $\|d\gamma_y\| = 1$ for all $y \in \mathcal{C}$ (for, if that isn't the case, we may replace $\gamma(y)$ by $\gamma(y)/\|d\gamma_y\|$, whose differential has unit norm on $\mathcal{C}$).

Being Jordan and smooth, the curve $\mathcal{C}$ is diffeomorphic to the set $S^1 := \mathbb{R} \bmod L$, and the diffeomorphism between the two sets is produced as follows. Since $\tilde{\sigma}$ is L-periodic, any two points t and $t + L$ in the domain of $\tilde{\sigma}$ can be identified. We define a map $\sigma : S^1 \to \mathbb{R}^2$ through the identity $\sigma([t]_L) = \tilde{\sigma}(t)$ for all $t \in \mathbb{R}$. Now σ maps S^1 diffeomorphically onto $\mathcal{C}$, and it has the same properties of $\tilde{\sigma}$: $\operatorname{Im}(\sigma) = \mathcal{C}$, $\|\sigma'(\cdot)\| \equiv 1$. Let $\varphi(\theta) : S^1 \to \mathbb{R} \bmod 2\pi$ be the map associating to each θ the angle of the tangent vector $\sigma'(\theta)$ to $\mathcal{C}$ at $\sigma(\theta)$. Then, the derivative φ' is the signed curvature of $\mathcal{C}$. Throughout this paper, we restrict the geometry of $\mathcal{C}$ by means of the next assumption.

Assumption 1 (Curve geometry)**.**

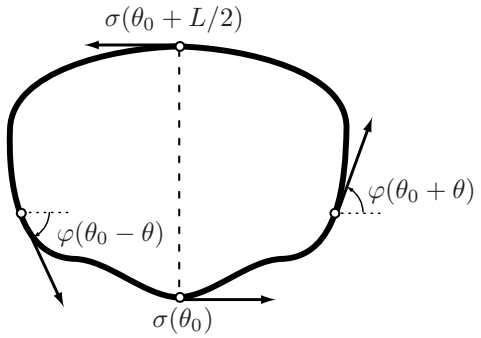

Fig. 1. An illustration of Assumption 1(i).

(i) There exists $\theta_0 \in S^1$ such that

$$\varphi(\theta_0 + \theta) = -\varphi(\theta_0 - \theta), \text{ for all } \theta \in S^1. \tag{2}$$

(ii) The curvature satisfies the inequality

$$|\varphi'(\theta)| < \sqrt{\left(\frac{2\pi}{L}\right)^2 + \left(\frac{\mu}{\epsilon}\right)^2} \text{ for all } \theta \in S^1. \tag{3}$$

Note that the identity in (2) holds modulo 2π. Assumption 1(i) implies that $\varphi(\theta_0) = [0]_{2\pi}$ and that

$$\begin{aligned} \sigma_1(\theta_0 + \theta) - \sigma_1(\theta_0) &= -\left(\sigma_1(\theta_0 - \theta) - \sigma_1(\theta_0)\right) \\ \sigma_2(\theta_0 + \theta) - \sigma_2(\theta_0) &= \sigma_1(\theta_0 - \theta) - \sigma_1(\theta_0), \end{aligned}$$

where σ_1 and σ_2 are the components of the map σ. Therefore, part (i) requires $\mathcal{C}$ to have a vertical symmetry axis passing through the point $\sigma(\theta_0)$. In particular, then, $\varphi(\theta_0 + L/2) = [\pi]_{2\pi}$. See Figure 1.

Remark 2.1. In the special case when $\mathcal{C}$ is a circle of length L, radius $L/(2\pi)$, and unit speed parameterization

$$\sigma(\theta) = \frac{L}{2\pi} \operatorname{col}\left(\cos\left(\frac{2\pi}{L}\theta\right), \sin\left(\frac{2\pi}{L}\theta\right)\right),$$

the assumption is satisfied with $\theta_0 = [-L/4]_L$. We verify this claim by computing the tangent vector to the circle at a point $\sigma(\theta)$, $\sigma'(\theta) = (-\sin(2\pi\theta/L), \cos(2\pi\theta/L))$ and its angle, $\varphi(\theta) = [(2\pi/L)\theta + \pi/2]_{2\pi}$. Now note that $\varphi([-L/4]_L) = [0]_{2\pi}$, and $\varphi'(\theta) = 2\pi/L$, which clearly satisfies identity (2) and bound (3). We will return to the circle at various times in the paper to illustrate our solution.

As seen above, the curvature of a circle of length L is $2\pi/L$. Thus, part (ii) of the assumption requires that the maximum curvature of $\mathcal{C}$ be not too much higher than that of a circle of the same length. In intuitive terms, the assumption limits the amount of deformation that one must apply to a circle in order to obtain $\mathcal{C}$. The higher the ratio μ/ϵ is, the more the maximum curvature of $\mathcal{C}$ can deviate from that of a circle of the same length, and hence the more deformation one may apply to the circle to obtain $\mathcal{C}$.

Path Following Problem (PFP): Given a Jordan curve $\sigma : S^1 \to \mathbb{R}^2$, with $\operatorname{Im}(\sigma) = \mathcal{C}$, satisfying Assumption 1, find a continuous feedback $u(x) = \operatorname{col}(u_1(x), u_2(x)) : M \to \mathbb{R}^2$ and an open set of initial conditions $U \subset M$ such that $\mathcal{C} \subset h(U)$, and the closed-loop system meets the following goals:

- **G1** For each initial condition in U, at least one solution $x(t)$ to (1) exists for all $t \geq 0$ and all solutions are such that $\|h(x(t))\|_{\mathcal{C}} \to 0$ in finite time.
- **G2** The set $\mathcal{C}$ is *output invariant* for the closed-loop system. In other words, if the centre of mass (x_1, x_3) is initialized on $\mathcal{C}$, and if the velocity vector (x_2, x_4) is initialized tangent to $\mathcal{C}$, then all solutions of the closed-loop system give output signals $y(t) \in \mathcal{C}$ for all $t \geq 0$.
- **G3** For each initial condition in U, there exists a time $T_1 > 0$ such that after time T_1, all output signals $y(t)$ trace the entire curve $\mathcal{C}$, i.e., $\operatorname{Im}(y([T_1, +\infty))) = \mathcal{C}$, in a desired direction and the speed $\|\dot{y}(t)\|$ is bounded away from zero.

G4 For each initial condition in U, there exists a time $T_2 > T_1$ after which the roll angle oscillates around its zero value, and its time average is zero. In other words, the aircraft does not undergo multiple revolutions about its longitudinal axis and, on average, its wings are parallel to the ground.

The reason for allowing continuous feedback, and therefore non-unique solutions, is that, in solving PFP, we will utilize the finite-time stabilization theory of [2], [3]. As mentioned in the introduction, goal **G2** is a crucial feature that distinguishes our control strategy from other path following control approaches in the literature and has considerable practical value. To illustrate its importance, suppose that a sudden disturbance slows down the PVTOL or even stops its motion without making its centre of mass abandon $\mathcal{C}$. If goal **G2** is met, then as soon as the disturbance vanishes, the PVTOL resumes its normal operation without leaving $\mathcal{C}$. On the other hand, a controller not meeting goal **G2** may have the undesirable property of making the PVTOL leave $\mathcal{C}$.

Our approach to solving PFP is summarized in the following steps.

(1) We find the four-dimensional *path following submanifold* $\Gamma_1^\star$ associated with $\mathcal{C}$ (see [16], [17]), i.e., the maximal controlled invariant subset of $h^{-1}(\mathcal{C})$. Physically, the set $\Gamma_1^\star$ is the collection of all those motions of the PVTOL system (1) whose associated output signal can be made to lie in $\mathcal{C}$ at all times by a suitable choice of input signal.
(2) We decompose system (1) into subsystems *tangential* and *transversal* to $\Gamma_1^\star$, with the property that the transversal subsystem is linear time invariant (LTI). The tangential and transversal subsystems are driven by tangential and transversal control inputs, $v^{\parallel}$ and $v^{\pitchfork}$, respectively.
(3) Using the theory of [2], we design the transversal controller $v^{\pitchfork}$ to finite-time stabilize the origin of the transversal subsystem. This controller meets goals **G1** and **G2**.
(4) We find a two-dimensional controlled invariant submanifold $\Gamma_2^\star \subset \Gamma_1^\star$, henceforth called the *roll dynamics manifold*, on which the roll dynamics (subsystem with state (x_5, x_6)) meet goal **G4**. More precisely, for all initial conditions on $\Gamma_2^\star$, the resulting roll angle, $x_5(t)$, is a periodic function with zero mean and its total variation is bounded. On $\Gamma_2^\star$, the PVTOL is subject to a virtual constraint: its centre of mass lies on $\mathcal{C}$, and its roll angle is entirely determined by the position of the PVTOL on $\mathcal{C}$.
(5) We design the tangential controller $v^{\parallel}$ to finite-time stabilize the roll dynamics submanifold $\Gamma_2^\star$.
(6) We show that the two-dimensional dynamics on $\Gamma_2^\star$ are Hamiltonian with energy $\mathcal{H} = T + V$ given by kinetic plus potential energy. Using this fact, we are able to completely characterize the motion on $\Gamma_2^\star$. In particular, we show that there exist two open subsets of $\Gamma_2^\star$ corresponding to clockwise and counterclockwise motion of the PVTOL on the curve $\mathcal{C}$, thus satisfying goal **G3**.

3 Solution of PFP

In this section we carry out in detail each point of the program outline above.

3.1 Step 1: Finding the path following manifold

In general, the path following manifold $\Gamma_1^\star$ associated with the curve $\mathcal{C}$ (see [16], [17]) is defined to be the maximal controlled invariant submanifold (if it exists) contained in $h^{-1}(\mathcal{C}) = \{x \in M : \gamma(\mathrm{col}(x_1, x_3)) = 0\}$. As such, $\Gamma_1^\star$ is the collection of all possible motions generated by the control system with the property that their associated outputs lie in $\mathcal{C}$ at all times. Equivalently, $\Gamma_1^\star$ is the zero dynamics manifold of (1) with output function $\tilde{h}(x) := \gamma(\mathrm{col}(x_1, x_3))$. In order to characterize $\Gamma_1^\star$ for the problem at hand, it suffices to notice that $\tilde{h}$ yields a well-defined relative degree 2 everywhere on $h^{-1}(\mathcal{C})$, since $L_{g_i}\tilde{h}(x) = 0$, for $i = 1, 2$ and for all $x \in M$, and

$$[L_{g_1}L_f\tilde{h} \quad L_{g_2}L_f\tilde{h}] = d\gamma_{(x_1,x_3)} \begin{bmatrix} -\sin x_5 & \epsilon\cos x_5 \\ \cos x_5 & \epsilon \sin x_5 \end{bmatrix}$$

has full rank 1 for all x in $h^{-1}(W)$. Therefore, the path following submanifold of (1) associated with $\mathcal{C}$ is the four-dimensional submanifold

$$\begin{aligned} \Gamma_1^\star &:= \{x \in M : \tilde{h}(x) = 0,\ L_f\tilde{h} = 0\} \\ &= \{x : \gamma(\mathrm{col}(x_1, x_3)) = 0, (\partial_{x_1}\gamma)x_2 + (\partial_{x_3}\gamma)x_4 = 0\}. \end{aligned} \tag{4}$$

Remark 3.1. When $\mathcal{C}$ is a circle of length L centred at the origin, the path following manifold can be expressed as

$$\Gamma_1^\star = \Big\{ x \in M : \frac{\pi}{L}\left(x_1^2 + x_3^2\right) - \frac{L}{4\pi} = 0, \\ \frac{2\pi}{L}\left(x_1 x_2 + x_3 x_4\right) = 0 \Big\}.$$

3.2 Step 2: Decomposition into transversal and tangential subsystems

We have established that $\Gamma_1^\star$ is the zero dynamics manifold associated with the output function $\tilde{h}$, and that $\tilde{h}$ yields relative degree 2. Now we perform input-output feedback linearization in a neighborhood of $\Gamma_1^\star$. To this end, define the partial coordinate transformation

$$\xi_1 = \tilde{h}(x) = \gamma(\mathrm{col}(x_1, x_3)) \\ \xi_2 = L_f \tilde{h}(x) = d\gamma_{\mathrm{col}(x_1,x_3)}(\mathrm{col}(x_2, x_4)).$$

Roughly speaking, ξ_1 is a measure of the distance of the point (x_1, x_3) to the curve $\mathcal{C}$, while ξ_2 is a measure of the velocity of $(x_1(t), x_3(t))$ relative to $\mathcal{C}$. Together, (ξ_1, ξ_2) represent transversal coordinates to $\Gamma_1^\star$. We need to find four functions completing the coordinate transformation. The states x_5 and x_6 are two obvious choices because they are functionally independent from ξ_1 and ξ_2. If, given $y \in \mathbb{R}^2$, we define

$$\pi(y) := \arg\min_{\theta \in S^1} \|y - \sigma(\theta)\|,$$

then $\theta = \pi(y)$ is such that the point $\sigma(\theta)$ is the orthogonal projection of y onto $\mathcal{C}$. Such a projection is unique in a neighborhood of $\mathcal{C}$, and in fact the tubular neighborhood theorem (see [8]) implies that there exists a sufficiently small constant $\varepsilon > 0$ such that, letting $\mathcal{C}^\varepsilon := \{y \in \mathbb{R}^2 : \|y\|_{\mathcal{C}} < \varepsilon\}$, the map $\pi : \mathcal{C}^\epsilon \to S^1$ defined above is smooth and, for all $y \in \mathcal{C}^\varepsilon$, $d\pi_y \neq 0$. The orthogonal projection map $\pi(y)$ and its time derivative are the two remaining functions we were looking for. In order to prove this claim, we need the following.

Lemma 3.2. For each $y \in \mathcal{C}$, the matrix

$$D(y) := \begin{bmatrix} d\pi_y \\ d\gamma_y \end{bmatrix} = \begin{bmatrix} \partial_{y_1}\pi & \partial_{y_2}\pi \\ \partial_{y_1}\gamma & \partial_{y_2}\gamma \end{bmatrix} \tag{5}$$

is orthogonal.

Proof. To begin with, by the definition of π, for any $\theta \in S^1$ and any $y \in \pi^{-1}(\theta)$, we have $\langle y - \sigma(\theta), \sigma'(\theta)\rangle = 0$. Therefore, recalling that $\sigma'(\theta)$ is the tangent vector to $\mathcal{C}$ at $\sigma(\theta)$, the set $\{y \in \mathcal{C}^\varepsilon : \pi(y) = \theta\}$ is a straight line segment through $\sigma(\theta)$, perpendicular to $\mathcal{C}$. Hence, the normal vector to this segment at $\sigma(\theta)$, $(d\pi_{\sigma(\theta)})^\top$, is tangent to $\mathcal{C}$, so $(d\pi_{\sigma(\theta)})^\top = k\,\sigma'(\theta)$, for some $k \in \mathbb{R}$. To find k, we differentiate the identity $\pi(\sigma(\theta)) = \theta$ with respect to θ, to obtain $d\pi_{\sigma(\theta)}(\sigma'(\theta)) = 1$, so that $k = 1$ and $(d\pi_{\sigma(\theta)})^\top = \sigma'(\theta)$. Since $\sigma(\theta)$ has unit norm, so does $d\pi_{\sigma(\theta)}$. On the other hand, differentiating the identity $\gamma \circ \sigma(\theta) \equiv 0$ with respect to θ we obtain $d\gamma_{\sigma(\theta)}(\sigma'(\theta)) = 0$, and so the vector $(d\gamma_{\sigma(\theta)})^\top$ is perpendicular to $\mathcal{C}$ at $\sigma(\theta)$. Moreover, by assumption this vector has unit norm. In conclusion, for each $y \in \mathcal{C}$, the vectors $d\pi_y$ and $d\gamma_y$ have unit norm and are perpendicular to each other. □

Lemma 3.3. The coordinate transformation

$$T : x \mapsto (\eta_1, \eta_2, \eta_3, \eta_4, \xi_1, \xi_2) \in (\mathbb{R} \bmod 2\pi) \times \mathbb{R} \times S^1 \times \mathbb{R}^3$$

defined as

$$\begin{bmatrix}\eta_1\\ \eta_2\\ \eta_3\\ \eta_4\\ \xi_1\\ \xi_2\end{bmatrix} := \begin{bmatrix} x_5 \\ x_6 \\ \pi(\mathrm{col}(x_1, x_3)) \\ d\pi_{\mathrm{col}(x_1,x_3)}(\mathrm{col}(x_2, x_4)) \\ \gamma(\mathrm{col}(x_1, x_3)) \\ d\gamma_{\mathrm{col}(x_1,x_3)}(\mathrm{col}(x_2, x_4))\end{bmatrix}, \tag{6}$$

is a diffeomorphism of a neighborhood V of $\Gamma_1^\star$ onto its image.

Proof. According to the generalized inverse function theorem (see [8, p.56]), it suffices to show that

(i) for all $x \in \Gamma_1^\star$, dT_x is an isomorphism, and
(ii) $T|_{\Gamma_1^\star} : \Gamma_1^\star \to T(\Gamma_1^\star)$ is a diffeomorphism.

For each $x \in \Gamma_1^\star$, dT_x has the matrix representation,

$$\begin{bmatrix} 0 & 0 & 0 & 0 & 1 & 0 \\ 0 & 0 & 0 & 0 & 0 & 1 \\ \partial_{x_1}\pi & 0 & \partial_{x_3}\pi & 0 & 0 & 0 \\ \star & \partial_{x_1}\pi & \star & \partial_{x_3}\pi & 0 & 0 \\ \partial_{x_1}\gamma & 0 & \partial_{x_3}\gamma & 0 & 0 & 0 \\ \star & \partial_{x_1}\gamma & \star & \partial_{x_3}\gamma & 0 & 0 \end{bmatrix},$$

where stars denote don't care elements. By Lemma 3.2, the matrix above is nonsingular, and so dT_x is an isomorphism on $\Gamma_1^\star$. To show that property (ii) holds, note that $\pi|_{\Gamma_1^\star} = \sigma^{-1}$, and consider the restriction of T to $\Gamma_1^\star$,

$$T|_{\Gamma_1^\star}(x) = \begin{bmatrix} x_5 \\ x_6 \\ \sigma^{-1}(\mathrm{col}(x_1, x_3)) \\ d\pi_{\mathrm{col}(x_1,x_3)}(\mathrm{col}(x_2, x_4)) \\ 0 \\ 0 \end{bmatrix}.$$

The map above is smooth and injective. Its inverse is given by the relationships $\mathrm{col}(x_1, x_3) = \sigma(\eta_3)$, $\mathrm{col}(x_2, x_4) = D^{-1}(\sigma(\eta_3)) \cdot \mathrm{col}(\eta_4, 0)$, and $\mathrm{col}(x_5, x_6) = \mathrm{col}(\eta_1, \eta_2)$, where $D(\cdot)$ is defined in (5), and is clearly smooth, proving that $T|_{\Gamma_1^\star}$ is a diffeomorphism onto its image. □

Example 3.4. Let $\mathcal{C}$ be a circle or radius L centred at the origin. Then, $\pi(y) = \frac{L}{2\pi}\arg(y_1 + i\, y_2)$. This function is smooth everywhere except at the origin. Next, we pick $\gamma(y)$ to be $\gamma(y) = (\pi/L)(y_1^2 + y_2^2) - L/(4\pi)$ so that, on $\mathcal{C}$, $\|d\gamma_y\| = 1$. On $\mathcal{C}$, D is given by

$$D(y) = \frac{2\pi}{L}\begin{bmatrix} -\,y_2 & y_1 \\ y_1 & y_2 \end{bmatrix},$$

and since $y_1^2 + y_2^2 = (L/(2\pi))^2$, we have that D is orthogonal, as predicted by Lemma 3.2. The coordinate transfor-

mation of Lemma 3.3 reads as

$$\begin{bmatrix}\eta_1\\ \eta_2\\ \eta_3\\ \eta_4\\ \xi_1\\ \xi_2\end{bmatrix} = \begin{bmatrix} x_5 \\ x_6 \\ \frac{L}{2\pi}\arg\left(x_1+ix_3\right) \\ \frac{L}{2\pi\left(x_1^2+x_3^2\right)}\left(x_1x_4-x_2x_3\right) \\ \frac{\pi}{L}\left(x_1^2+x_3^2\right)-\frac{L}{4\pi} \\ \frac{2\pi}{L}\left(x_1x_2+x_3x_4\right)\end{bmatrix},$$

and the domain of the transformation is $M-\{x : x_1 = x_3 = 0\}$.

We now return to the general situation and apply the coordinate transformation (6) to (1) to get

$$\begin{aligned}
\dot\eta_1 &= \eta_2\\
\dot\eta_2 &= \mu\, u_2\\
\dot\eta_3 &= \eta_4\\
\dot\eta_4 &= \dot{d\pi}\ \mathrm{col}(x_2,x_4) - g\,\partial_{x_3}\pi + d\pi_{\mathrm{col}(x_1,x_3)}R(x_5)\begin{bmatrix}u_1\\u_2\end{bmatrix}\\
\dot\xi_1 &= \xi_2\\
\dot\xi_2 &= \dot{d\gamma}\ \mathrm{col}(x_2,x_4) - g\,\partial_{x_3}\gamma + d\gamma_{\mathrm{col}(x_1,x_3)}R(x_5)\begin{bmatrix}u_1\\u_2\end{bmatrix},
\end{aligned}$$

where $\dot{d\pi}$ and $\dot{d\gamma}$ are the time derivatives of the row vectors $d\pi_{\mathrm{col}(x_1,x_3)}$ and $d\gamma_{\mathrm{col}(x_1,x_3)}$ along the vector field f, and

$$R(x_5) = \begin{bmatrix} -\sin x_5 & \epsilon\cos x_5 \\ \cos x_5 & \epsilon\sin x_5\end{bmatrix}.$$

Since $d\pi_{\mathrm{col}(x_1,x_3)}$ and $d\gamma_{\mathrm{col}(x_1,x_3)}$ are linearly independent on $\Gamma_1^\star$, they remain so in a neighborhood of $\Gamma_1^\star$, without loss of generality on V. Consider the regular feedback transformation on V,

$$\begin{aligned}\begin{bmatrix}u_1\\u_2\end{bmatrix} := R^{-1}(x_5)D^{-1}(\mathrm{col}(x_1,x_3))\Bigg(&-\begin{bmatrix}\dot{d\pi}\\ \dot{d\gamma}\end{bmatrix}\mathrm{col}(x_2,x_4)\\ &+ g\begin{bmatrix}\partial_{x_3}\pi\\ \partial_{x_3}\gamma\end{bmatrix} + \begin{bmatrix}v^{\parallel}\\ v^{\pitchfork}\end{bmatrix}\Bigg),\end{aligned} \tag{7}$$

where $v^{\parallel}$ and $v^{\pitchfork}$ are new control inputs. The PVTOL after coordinate and feedback transformation reads as

$$\begin{aligned}
\dot\eta_1 &= \eta_2\\
\dot\eta_2 &= \mu\, u_2(\eta_1,\eta_3,\xi_1,v^{\parallel},v^{\pitchfork})\\
\dot\eta_3 &= \eta_4\\
\dot\eta_4 &= v^{\parallel}\\
\dot\xi_1 &= \xi_2\\
\dot\xi_2 &= v^{\pitchfork}.
\end{aligned} \tag{8}$$

In (η,ξ) coordinates, the path following manifold is given by $T(\Gamma_1^\star) = \{(\eta,\xi) : \xi = 0\}$. Therefore, the ξ subsystem describes the dynamics of the PVTOL transversal to $\Gamma_1^\star$, and for this reason it is called the *transversal subsystem*, driven by the *transversal input* $v^{\pitchfork}$. On the other hand, the restriction of the η subsystem to $T(\Gamma_1^\star)$ when $v^{\pitchfork} = 0$ represents the dynamics of the PVTOL on $\Gamma_1^\star$, and is therefore referred to as the *tangential subsystem*, driven by the

tangential input $v^{\parallel}$. The decomposition of the PVTOL model into subsystems tangential and transversal to $\Gamma_1^\star$ and of the controls into tangential and transversal components is referred to as transverse feedback linearization [16], [18].

3.3 Step 3: Transversal control design

Since the transversal subsystem in (8) is a double integrator, we could stabilize it using a simple linear feedback $v^{\pitchfork}(\xi) = K\xi$. However, in order to simplify the stability analysis that follows, it is convenient to stabilize $\xi = 0$ in finite time. Following the work in [2], [3], we define a controller $v^{\pitchfork}(\xi)$ guaranteeing that trajectories of the ξ subsystem are stable and converge to zero in a finite time which is uniform over compact sets of initial conditions so that, in x coordinates, $\Gamma_1^\star$ is locally stabilized in finite time, meeting goals **G1** and **G2**. The controller in question is given by

$$v^{\pitchfork}(\xi) = -\frac{1}{k_1}\left(\operatorname{sgn}(k_1\xi_2)|k_1\xi_2|^{\frac{1}{2}} + \operatorname{sgn}(\phi(\xi))|\phi(\xi)|^{\frac{1}{3}}\right), \tag{9}$$

where $k_1 > 0$ is a design parameter, and

$$\phi(\xi) := k_1\xi_1 + \frac{2}{3}\operatorname{sgn}(k_1\xi_2)|k_1\xi_2|^{\frac{3}{2}}.$$

A control law analogous to $v^{\pitchfork}(\xi)$ is used in [21] and is based on the controllers introduced in [2]. The control law (9) globally asymptotically stabilizes ξ. Furthermore, there exists a continuous function $T_\xi(\zeta, k_1)$, $[0,+\infty)\times[0,+\infty) \to [0,+\infty)$, with the following properties:

(i) For all $\|\xi(0)\| < \zeta$, $\xi(t) = 0$ for all $t \geq T_\xi(\zeta, k_1)$.
(ii) $T_\xi(\zeta, k_1) \to 0$ as $k_1 \to 0^+$, and $T_\xi(0, k_1) = 0$.

The existence and properties of T_ξ follow from the proof of Proposition 1 in [2], and utilizes [3, Theorem 4.2].

3.4 Step 4: Finding the roll dynamics submanifold

In this section we consider the motion of the PVTOL on the path following manifold $\Gamma_1^\star$. In light of the results of the previous section, for all t greater than $T_\xi(\|\xi(0)\|, k_1)$, we have $\xi(t) = 0$ and therefore also $v^{\pitchfork}(t) = 0$. Therefore, the motion on the path following manifold $\Gamma_1^\star$ is determined by setting $\xi = 0$ and $v^{\pitchfork} = 0$ in (8).

Lemma 3.5. The tangential subsystem on $\Gamma_1^\star$, obtained from (8) by setting $\xi = 0$ and $v^{\pitchfork} = 0$, is given by

$$\begin{aligned}
\dot\eta_1 &= \eta_2\\
\dot\eta_2 &= \frac{\mu}{\epsilon}(g\sin\eta_1 + \sin(\eta_1 - \varphi(\eta_3))\varphi'(\eta_3)\eta_4^2\\
&\qquad + \cos(\eta_1 - \varphi(\eta_3))v^{\parallel})\\
\dot\eta_3 &= \eta_4\\
\dot\eta_4 &= v^{\parallel}.
\end{aligned} \tag{10}$$

Proof. On $\Gamma_1^\star$, and setting $v^{\pitchfork} = 0$, the matrix D is orthogonal and the control u_2 in the feedback transformation (7) is given by

$$\begin{aligned}
u_2 =& \frac{1}{\epsilon}[\cos\eta_1 \quad \sin\eta_1][\nabla\pi \quad \nabla\gamma]\left(-\begin{bmatrix} \dot{d\pi}\\ \dot{d\gamma}\end{bmatrix}\operatorname{col}(x_2, x_4)\right.\\
&\left. + g\begin{bmatrix}\partial_{x_3}\pi\\ \partial_{x_3}\gamma\end{bmatrix} + \begin{bmatrix} v^{\parallel}\\ 0\end{bmatrix}\right).
\end{aligned}$$

Recall that $d\pi_{\operatorname{col}(x_1,x_3)}$ and $d\gamma_{\operatorname{col}(x_1,x_3)}$ are two orthonormal vectors. Moreover, we have shown in the proof of Lemma 3.2 that $(d\pi_{\sigma(\theta)})^\top = \sigma'(\theta)$, and so in η coordinates, when $\xi = 0$, we have $d\pi_{\operatorname{col}(x_1,x_3)} = [\cos\varphi(\eta_3) \quad \sin\varphi(\eta_3)]$, $d\gamma_{\operatorname{col}(x_1,x_3)} = [\sin\varphi(\eta_3) \quad -\cos\varphi(\eta_3)]$, and $\dot{d\pi} = \varphi'(\eta_3)\eta_4\,[-\sin\varphi(\eta_3) \quad \cos\varphi(\eta_3)]$, $\dot{d\gamma} = \varphi'(\eta_3)\eta_4\,[\cos\varphi(\eta_3) \quad \sin\varphi(\eta_3)]$. Finally, on $\Gamma_1^\star$ we have $\operatorname{col}(x_2, x_4) = D(\sigma(\eta_3))^{-1}\operatorname{col}(\eta_4, 0) = \eta_4\nabla\pi = \eta_4\operatorname{col}(\cos\varphi(\eta_3), \sin\varphi(\eta_3))$. Using the identities above in the expression for u_2, we obtain the differential equation (10). □

Next, in order meet goal **G4**, we will impose a "virtual constraint" for the roll angle η_1, $\eta_1 = f(\eta_3)$, where $f : S^1 \to \mathbb{R} \bmod 2\pi$ is a function to be determined to fulfill the two objectives:

(i) f is a well-defined smooth function $S^1 \to \mathbb{R} \bmod 2\pi$. In other words, there exists an L-periodic smooth function $\tilde{f} : \mathbb{R} \to \mathbb{R} \bmod 2\pi$ such that $f([x]_L) = \tilde{f}(x)$ for all $x \in \mathbb{R}$;
(ii) f is odd with respect to θ_0, i.e., $f(\theta_0 + \eta_3) = -f(\theta_0 - \eta_3)$ for all $\eta_3 \in S^1$.

The constraint $\eta_1 = f(\eta_3)$ will identify a submanifold $\Gamma_2^\star \subset \Gamma_1^\star$. We will show in Section 3.6 that meeting objective (ii) above guarantees that each solution $(\eta_3(t), \eta_4(t))$ on $\Gamma_2^\star$ is such that the signal $\eta_1(t) = f(\eta_3(t))$ oscillates around $\eta_1 = 0$ and has time average zero, as required by goal **G4**.

The design of the virtual constraint f is key to our path following solution. The use of virtual holonomic constraints for control design in Euler-Lagrange systems underactuated by one control was investigated in [25]. The work in [7] is also related to our approach because there the authors design an output function to ensure that the resulting zero-dynamics are orbitally stable.

In order for $\eta_1 = f(\eta_3)$ to be a feasible constraint for (10), we need

$$\begin{aligned}\dot{\eta}_1 &= \eta_2 = f'(\eta_3)\eta_4\\ \ddot{\eta}_1 &= \dot{\eta}_2 = f''(\eta_3)\eta_4^2 + f'(\eta_3)v^{\parallel}.\end{aligned}$$

Thus, if

$$\begin{aligned}&\frac{\mu}{\epsilon}\left(g\sin\eta_1 + \sin(\eta_1-\varphi)\varphi'\eta_4^2 + \cos(\eta_1-\varphi)v^{\parallel}\right)\Big|_{\eta_1=f(\eta_3)}\\ &= f''(\eta_3)\eta_4^2 + f'(\eta_3)v^{\parallel},\end{aligned}$$

then the two-dimensional submanifold

$$T(\Gamma_2^\star) := \{(\eta,\xi) : \eta_1 = f(\eta_3), \eta_2 = f'(\eta_3)\eta_4, \xi = 0\} \tag{11}$$

is controlled invariant. Solving the above equation for $v^{\parallel}$, we obtain

$$\begin{aligned}v^{\parallel} = \frac{\mu/\epsilon}{f'(\eta_3) - \frac{\mu}{\epsilon}\cos(f(\eta_3)-\varphi(\eta_3))}\Big(&g\sin f(\eta_3)\\ &+ [\sin(f(\eta_3)-\varphi(\eta_3))\varphi'(\eta_3) - \frac{\epsilon}{\mu}f''(\eta_3)]\eta_4^2\Big).\end{aligned} \tag{12}$$

The feedback $v^{\parallel}$ is smooth if its denominator is bounded away from zero. If there exists a function f satisfying properties (i) and (ii) above, and such that, for all $\eta_3 \in S^1$, $f'(\eta_3) - \frac{\mu}{\epsilon}\cos(f(\eta_3)-\varphi(\eta_3)) \neq 0$, then on the corresponding controlled invariant set $\Gamma_2^\star$ defined by (11), the system meets goal **G4**. Note that there may be many choices of f yielding the desired result. We find one such function by imposing that

$$f'(\eta_3) = \frac{\mu}{\epsilon}\cos(f(\eta_3)-\varphi(\eta_3)) + \varphi'(\eta_3) - \delta_0, \tag{13}$$

where δ_0 is a positive constant yet to be specified such that the denominator of (12) is bounded away from zero on $\Gamma_2^\star$, i.e., $|\varphi'(\eta_3) - \delta_0| > 0$ for all $\eta_3 \in S^1$. Letting $\lambda := f - \varphi$, the above equation becomes

$$\lambda' = \frac{\mu}{\epsilon}\cos\lambda - \delta_0,$$

where prime indicates differentiation with respect to η_3. The above is a first-order ODE on S^1 which we now explicitly solve. We begin by assuming that λ is a real variable, in which case the solutions are

$$\lambda(x) = -\frac{\pi}{2} + 2\arctan\left(\frac{1}{\delta_0}\left(\alpha\tan\left(\frac{\alpha}{2}(K-x)\right) + \frac{\mu}{\epsilon}\right)\right),$$

where $\alpha = \sqrt{\delta_0^2 - \left(\frac{\mu}{\epsilon}\right)^2}$ and K is the integration constant. Notice $\lambda(x)$ has 2π jumps whenever the argument of $\tan(\cdot)$ is $\pm\pi/2$, but $[\lambda(x)]_{2\pi}$ is a smooth function. Next, in order to guarantee that $[\lambda(x)]_{2\pi}$ is L-periodic, we impose that $\alpha/2 = \pi/L$, or

$$\delta_0 = \sqrt{\left(\frac{2\pi}{L}\right)^2 + \left(\frac{\mu}{\epsilon}\right)^2}. \tag{14}$$

With this choice of δ_0, the function $\tilde{f}(x) := \left[\varphi([x]_L) + \lambda(x)\right]_{2\pi}$ is L-periodic because it is the sum of two L-periodic functions. The periodicity of $\tilde{f}$ allows us to define $f(\eta_3)$ by replacing the argument x by η_3 in $\tilde{f}$,

$$\begin{aligned} f(\eta_3) = [\varphi(\eta_3) + \lambda(\eta_3)]_{2\pi} = \Bigg[\varphi(\eta_3) - \frac{\pi}{2} \\ + 2\arctan\left(\frac{1}{\delta_0}\left(\frac{2\pi}{L}\tan\left(\frac{\pi}{L}(K-\eta_3)\right) + \frac{\mu}{\epsilon}\right)\right)\Bigg]_{2\pi}, \end{aligned} \tag{15}$$

so that $\tilde{f}(x) = f([x]_L)$ for all $x \in \mathbb{R}$ (property (i)). The function $f(\eta_3)$ is smooth, well-defined on S^1, and satisfies (13). Moreover, by inequality (3) in Assumption 1, the choice of δ_0 above yields $|\varphi'(\eta_3) - \delta_0| > 0$ for all $\eta_3 \in S^1$, and so the feedback $v^{\parallel}$ in (12) is smooth. Next, we choose the integration constant K in $\lambda(x)$ to ensure that f is odd with respect to θ_0 (property (ii)), which occurs when f' is even with respect to θ_0 and $f(\theta_0) = 0$. Letting

$$\bar{\eta}_3(K) := K - \frac{L}{\pi}\arctan\left(\frac{L\delta_0}{2\pi} - \frac{\mu L}{2\pi\epsilon}\right),$$

we have $\lambda(\bar{\eta}_3(K)) = 0$ and it is not hard to see that $\cos\lambda(\eta_3)$ is an even function with respect to $\bar{\eta}_3$, i.e., $\cos[\lambda(\bar{\eta}_3(K)+\eta_3)] = \cos[\lambda(\bar{\eta}_3(K) - \eta_3)]$. By Assumption 1, φ' is an even function with respect to θ_0. We choose K so that $\bar{\eta}_3(K) = \theta_0$, i.e.,

$$K = \frac{L}{\pi}\arctan\left(\frac{L\delta_0}{2\pi} - \frac{\mu L}{2\pi\epsilon}\right) + \theta_0, \tag{16}$$

so that $\cos\lambda(\eta_3)$ is now even with respect to θ_0. With this choice, from (13) we conclude that $f'(\eta_3)$ is even with respect to θ_0. Since

$$f(\theta_0) = \left[\varphi(\theta_0) + \lambda(\theta_0)\right]_{2\pi} = \left[\varphi(\theta_0) + \lambda(\bar{\eta}_3(K))\right]_{2\pi} = [0]_{2\pi}$$

and f' is even, we have that $f(\eta_3)$ is odd with respect to θ_0, i.e.,

$$f(\theta_0 + \eta_3) = -f(\theta_0 - \eta_3), \tag{17}$$

as required.

To summarize, picking K as in (16), the function $f : S^1 \to \mathbb{R} \bmod 2\pi$ given by (15), with δ_0 defined in (14), is smooth, L-periodic, and is odd with respect to θ_0. Moreover, the feedback $v^{\parallel}$ in (12) is smooth and renders the submanifold $\Gamma_2^\star \subset \Gamma_1^\star$ defined in (11) invariant. We call this submanifold the *roll dynamics manifold*. From a physical point of view, when the state of the PVTOL is on $\Gamma_2^\star$, the roll angle x_5 (equal to η_1) is completely determined by the position $\pi(y)$ (equal to η_3) of the aircraft on $\mathcal{C}$ by means of the virtual constraint $\eta_1 = f(\eta_3)$. Hence, no matter what the dynamics of the aircraft's centre of mass on $\mathcal{C}$ are, the roll angle does not perform multiple revolutions about its longitudinal axis.

Remark 3.6. If $\mathcal{C}$ is a circle of length L with counterclockwise orientation then, as seen earlier, $\varphi(\theta) = \left[\frac{2\pi}{L}\theta + \frac{\pi}{2}\right]_{2\pi}$ and $\theta_0 = [-L/4]_L$. Figure 2 illustrates the configuration of the PVTOL on the roll dynamics manifold when $\mu/\epsilon = 1$ and the circle has radius 1. The property of f being odd with respect to θ_0 is reflected in the symmetry of the configuration with respect to the vertical axis passing through the centre of the circle.

3.5 Step 5: Tangential control design

Having identified a submanifold $\Gamma_2^\star \subset \Gamma_1^\star$ on which the roll angle of the PVTOL exhibits desired properties, we use the tangential input $v^{\parallel}$ in (10) to stabilize $\Gamma_2^\star$. Define error variables $e_1 = \eta_1 - f(\eta_3)$, $e_2 = \eta_2 - f'(\eta_3)\eta_4$. On $\Gamma_1^\star$,

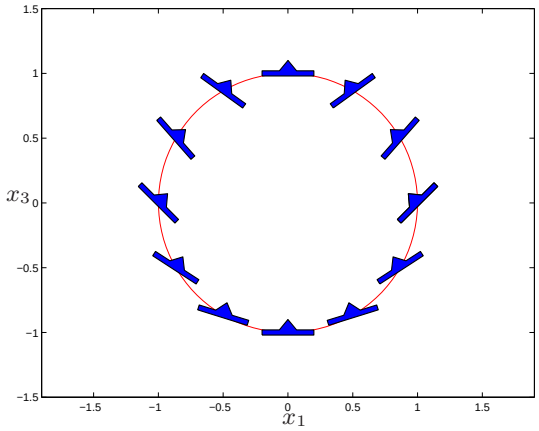

Fig. 2. Configuration of the PVTOL on the roll dynamics manifold, i.e., when $\eta_1 = f(\eta_3)$ and $\xi = 0$, for the case when $\mathcal{C}$ is the unit circle. Note the symmetry of the configuration with respect to the vertical axis passing through the centre of the circle.

stabilizing $\Gamma_2^\star$ is equivalent to stabilizing the origin of the error dynamics

$$\begin{aligned}\dot{e}_1 &= e_2\\ \dot{e}_2 &= \beta(\eta_1,\eta_3,\eta_4) - \left(f'(\eta_3) - \frac{\mu}{\epsilon}\cos(\eta_1 - \varphi(\eta_3))\right) v^{\parallel},\end{aligned}$$

where

$$\beta = \frac{\mu}{\epsilon}\left(g\sin\eta_1 + [\sin(\eta_1 - \varphi(\eta_3))\varphi'(\eta_3) - \frac{\epsilon}{\mu}f''(\eta_3)]\eta_4^2\right). \tag{18}$$

We pick the tangential controller on $\Gamma_1^\star$ to be

$$v^{\parallel}(\eta) = \frac{\beta(\eta_1,\eta_3,\eta_4) - w(e)}{f'(\eta_3) - \frac{\mu}{\epsilon}\cos(\eta_1 - \varphi(\eta_3))}, \tag{19}$$

where $w(e)$ is a continuous function chosen to finite-time stabilize the rotational (since e_1 is a variable in $\mathbb{R} \bmod 2\pi$) double integrator $\dot{e}_1 = e_2$, $\dot{e}_2 = w(e)$. The expression for $w(e)$ is a slight modification of the control law originally introduced in [2], and is given by

$$\begin{aligned}w(e) := -\frac{1}{k_2}\Big(&\operatorname{sgn}(k_2 e_2)|k_2 e_2|^{\frac{1}{2}}\\ &+ k_2^{\frac{1}{3}}\operatorname{sgn}(\sin(\psi(e)))\,|\sin(\psi(e))|^{\frac{1}{3}}\Big),\end{aligned} \tag{20}$$

where $k_2 > 0$ is a design parameter and

$$\psi(e) := e_1 + \frac{2}{3}k_2^{\frac{1}{2}}\operatorname{sgn}(e_2)\,|e_2|^{\frac{3}{2}}.$$

Remark 3.7. The tangential feedback $v^{\parallel}$ in (19) is well-defined on the subset of $\Gamma_1^\star$ where the denominator is bounded away from zero. On $\Gamma_2^\star \subset \Gamma_1^\star$, the denominator in question takes the form $f'(\eta_3) - (\mu/\epsilon)\cos(f(\eta_3) - \varphi(\eta_3))$ which, by our choice of f, is equal to $\varphi'(\eta_3) - \delta_0$ and is bounded away from zero for all η_3. Therefore, the denominator of (19) is bounded away from zero in a neighborhood of $\Gamma_2^\star$ in $\Gamma_1^\star$. An estimate of this neighborhood is found by noting that

$$\begin{aligned}f'(\eta_3) - \frac{\mu}{\epsilon}\cos(\eta_1 - \varphi(\eta_3)) &= \varphi'(\eta_3) - \delta_0\\ + \frac{\mu}{\epsilon}\left[\cos(\eta_1 - \varphi)(\cos e_1 - 1) + \sin(\eta_1 - \varphi)\sin e_1\right],&\end{aligned}$$

and thus the left-hand side is bounded away from zero for all those values of e_1 such that $(\mu/\epsilon)(|1-\cos e_1| + |\sin e_1|) < \min_{\eta_3 \in S^1}(\varphi'(\eta_3) - \delta_0)$. By (3), the right-hand side of this inequality is > 0.

The equilibrium $e = ([0]_{2\pi}, 0)$ of the rotational double integrator $\dot{e}_1 = e_2$, $\dot{e}_2 = w(e)$ with control law (20) is *not* globally finite-time stable [1], for the continuous control law introduces a saddle point at $e = ([\pi]_{2\pi}, 0)$. However, the equilibrium $e = ([0]_{2\pi}, 0)$ is almost globally finite-time stable, as for any initial condition on $S := \mathbb{R} \bmod 2\pi \times \mathbb{R} - \{e : \psi(e) = [\pi]_{2\pi}\}$ the solution converges to the equilibrium in question in finite time. Finally, there exists a continuous "settling time" function $T_e(\zeta, k_2)$, $[0, +\infty) \times [0, +\infty) \to [0, +\infty)$, with the following properties:

(i) For all $e(0) \in \Gamma_2^\star$ such that $\|e(0)\| < \zeta$, $e(t) = 0$ for all $t \geq T_e(\zeta, k_2)$.
(ii) $T_e(\zeta, k_2) \to 0$ as $k_2 \to 0^+$, and $T_e(0, k_1) = 0$.

Remark 3.8. We picked the tangential controller $v^\parallel$ in (19) to achieve desired properties for the roll dynamics on $\Gamma_1^\star$, namely to finite-time stabilize $\Gamma_2^\star$. As a result, the controller is only a function of η. While the transversal controller guarantees that $\Gamma_1^\star$ is reached in finite time, it may be desirable to modify $v^\parallel$ off of $\Gamma_1^\star$ to guarantee boundedness of the roll dynamics during the finite-time transient. This is certainly possible but we do not explore it in this paper.

3.6 Step 6: Motion on the roll dynamics manifold

So far we picked the transversal controller $v^\pitchfork(\xi)$ to locally finite-time stabilize the path following manifold $\Gamma_1^\star$ defined in (4), and the tangential controller $v^\parallel(\eta)$ to locally finite-time stabilize $\Gamma_2^\star$ from within $\Gamma_1^\star$. What is left is to do is to investigate the dynamics of the closed-loop system on the two dimensional submanifold $\Gamma_2^\star$. On $\Gamma_2^\star$, $v^\parallel$ is given by (12). Substituting that expression in (10) and setting $\eta_1 = f(\eta_3)$, $\eta_2 = f'(\eta_3)\eta_4$ we obtain the reduced second-order system describing the motion on the roll dynamics manifold $\Gamma_2^\star$,

$$\begin{aligned} \dot{\eta}_3 &= \eta_4 \\ \dot{\eta}_4 &= \phi_1(\eta_3) + \phi_2(\eta_3)\eta_4^2 \end{aligned} \tag{21}$$

where,

$$\begin{aligned} \phi_1(\eta_3) &= \frac{(\mu/\epsilon) g \sin f(\eta_3)}{\varphi'(\eta_3) - \delta_0} \\ \phi_2(\eta_3) &= \frac{(\mu/\epsilon) \sin(f(\eta_3) - \varphi(\eta_3))\varphi'(\eta_3) - f''(\eta_3)}{\varphi'(\eta_3) - \delta_0}. \end{aligned}$$

Physically, the dynamics in (21) describe the evolution of the position and velocity of the PVTOL's centre of mass along the curve $\mathcal{C}$. In order to meet goal **G3**, it is necessary for η_3 to traverse the entire S^1 (which corresponds to the PVTOL traversing the entire curve $\mathcal{C}$) in a desired direction while η_4 remains bounded. We will show that almost all phase curves of $\mathcal{C}$ can be of three types: equilibria, closed curves corresponding to oscillations (i.e., the PVTOL oscillates back and forth on a segment of $\mathcal{C}$ without traversing the entire $\mathcal{C}$), and closed curves corresponding to complete rotations around S^1. The latter is the type we are interested in, and we'll precisely characterize the domain of initial conditions of interest. The crucial realization to understanding the dynamics in (21) is that the system is Hamiltonian with energy function

$$\mathcal{H}(\eta_3, \eta_4) = \frac{1}{2} M(\eta_3)\eta_4^2 + V(\eta_3),$$

and canonical coordinates $(q, p) = (\eta_3, M(\eta_3)\eta_4)$. The functions M and V are given by

$$\begin{aligned} M(\eta_3) &= \exp\left(-2\int_0^{\eta_3} \phi_2(\tau) d\tau\right) \\ V(\eta_3) &= -\int_0^{\eta_3} \phi_1(\mu) M(\mu) d\mu. \end{aligned}$$

Note that $M'(\eta_3) = -2M(\eta_3)\phi_2(\eta_3)$ and $V'(\eta_3) = -M(\eta_3)\phi_1(\eta_3)$. Using these identities, it immediately follows that $\mathcal{H}$ is a first integral of (21). Moreover, it is easy to see that in (q, p) coordinates (21) takes on the canonical form of Hamilton's equations. However, in order for this discussion to make sense, we need to show that $M(\eta_3)$ and $V(\eta_3)$

[1] This is hardly surprising, as it is well-known that *no continuous control law* can globally stabilize an equilibrium on the cylinder.

are well-defined smooth functions on S^1. To this end, define $\tilde{M}, \tilde{V} : \mathbb{R} \to \mathbb{R}$ as

$$\tilde{M}(x) = \exp\left(-2\int_0^{[x]_L} \phi_2([\tau]_L)d\tau\right)$$
$$\tilde{V}(x) = -\int_0^{[x]_L} \phi_1([\mu]_L)\tilde{M}(\mu)d\mu,$$

and note that, for all $x \in \mathbb{R}$, $M([x]_L) = \tilde{M}(x)$ and $V([x]_L) = \tilde{V}(x)$.

Lemma 3.9. The functions $\tilde{M}(x)$ and $\tilde{V}(x)$ are smooth and L-periodic. Therefore, $M(\eta_3)$ and $V(\eta_3)$ are well-defined smooth functions $S^1 \to \mathbb{R}$.

Proof. We have shown in Section 3.4 that the function $x \mapsto f([x]_L) = \tilde{f}(x)$ is smooth. Since $f''([x]_L) = d^2 f([x]_L)/dx^2$, the function $x \mapsto f''([x]_L)$ is smooth as well. The map $x \mapsto \varphi([x]_L)$ is smooth because $\varphi([x]_L)$ is the angle of the tangent vector $\tilde{\sigma}'(x)$ ($\tilde{\sigma}$ was defined at the beginning of Section 2), and $\tilde{\sigma}'(x)$ is a smooth function. Analogously, the function $x \mapsto \varphi'([x]_L)$ is smooth. Since $\tilde{M}(x)$ and $\tilde{V}(x)$ result from integrating compositions of the functions above, $\tilde{M}(x)$ and $\tilde{V}(x)$ are smooth as well. Next, we turn our attention to the periodicity of $\tilde{M}$ and $\tilde{V}$. Obviously, the function $x \mapsto \phi_2([x]_L)$ is L-periodic. Therefore, the function $\tilde{M}(x)$ is L-periodic if and only if $\phi_2([x]_L)$ has zero mean. To show that $\phi_2([x]_L)$ has zero mean, it suffices to show that it is odd with respect to θ_0, which is true if and only if $\eta_3 \mapsto \phi_2(\eta_3)$ is odd with respect to θ_0. By assumption, $\varphi'(\eta_3)$ is even with respect to θ_0, and so $[\varphi'(\eta_3) - \delta_0]^{-1}$ is even as well. Therefore, to show that $\phi_2(\eta_3)$ is odd, it suffices to show that the numerator $(\mu/\epsilon)\sin(f(\eta_3) - \varphi(\eta_3))\varphi'(\eta_3) - f''(\eta_3)$ is odd with respect to θ_0. Since $f'(\eta_3)$ is even, $f''(\eta_3)$ is odd. Next, $\sin(f(\eta_3) - \varphi(\eta_3)) = \sin\lambda(\eta_3)$. Recall that, by our choice of K in (16), $\cos\lambda(\eta_3)$ is even with respect to θ_0, and so $\sin\lambda(\eta_3)$ is odd. When this function is multiplied by the even function φ', the result is an odd function with respect to θ_0, and so $\phi_2(\eta_3)$ is odd, as required. Next, we show that $\tilde{V}$ is L-periodic. Since $\phi_1([x]_L)$ and $\tilde{M}(x)$ are L-periodic, the function $\tilde{V}(x)$ is L-periodic if and only if the function $x \mapsto \phi_1([x]_L)\tilde{M}([x]_L)$ has zero mean. Once again, we show that this is the case by proving that $\phi_1([x]_L)\tilde{M}([x]_L)$ is odd or, what is the same, that $\phi_1(\eta_3)M(\eta_3)$ is odd. Since $\phi_2(\eta_3)$ is odd, the antiderivative $\int_0^{\eta_3}\phi_2(\tau)d\tau$ is even, and hence $M(\eta_3)$ is even as well. We are left to show that ϕ_1 is odd, and this follows from the fact that it is proportional to the ratio of an odd function, $\sin f(\eta_3)$, and an even one, $\varphi'(\eta_3) - \delta_0$. □

The next result characterizes the equilibria on the roll dynamics manifold, and their stability type.

Lemma 3.10. Consider the dynamics in (21) of the PVTOL on the roll manifold. The equilibria are pairs $(\eta_3^\star, 0)$ given by values of $\eta_3^\star$ such that either $f(\eta_3^\star) = [0]_{2\pi}$ or $f(\eta_3^\star) = [\pi]_{2\pi}$. There are at least two equilibria corresponding to $\eta_3^\star = \theta_0, \theta_0 + L/2$. The equilibrium at $(\theta_0 + L/2, 0)$ is always unstable. If there are only two equilibria, then the equilibrium at $(\theta_0, 0)$ is stable.

Proof. The equilibria are pairs $(\eta_3^\star, 0)$, where the values of $\eta_3^\star$ are the extrema of $V(\eta_3)$. We have $V'(\eta_3) = 0$ if and only if either $f(\eta_3^\star) = [0]_{2\pi}$ or $[\pi]_{2\pi}$. It can be shown that $f(\theta_0) = [0]_{2\pi}$ and $f(\theta_0 + L/2) = [0]_{2\pi}$ and so (21) has at least two equilibria, $(\theta_0, 0)$, and $(\theta_0 + L/2, 0)$. The stability type of each equilibrium $(\eta_3^\star, 0)$ is determined by whether $\eta_3^\star$ is a minimum (in which case the equilibrium is stable) or a maximum of V (in which case the equilibrium is unstable). For any extremum $\eta_3^\star$ of V, we have

$$V''(\eta_3^\star) = \frac{(\mu/\epsilon)M(\eta_3^\star)}{\delta_0 - \varphi'(\eta_3^\star)}\cos f(\eta_3^\star)f'(\eta_3^\star).$$

The function $M(\cdot)$ is always positive and, by (3), so is the denominator of V''. Hence, $\operatorname{sgn}(V''(\eta_3^\star)) = \operatorname{sgn}(\cos f(\eta_3^\star)f'(\eta_3^\star))$. Using this fact, relation (13), and the identities $\varphi(\theta_0) = [0]_{2\pi}$, $\varphi(\theta_0 + L/2) = [\pi]_{2\pi}$, we obtain

$$\begin{aligned}\operatorname{sgn}\left(V''(\theta_0 + L/2)\right) &= \operatorname{sgn}(f'(\theta_0 + L/2)) \\ &= \operatorname{sgn}(-(\mu/\epsilon) + \varphi'(\theta_0 + L/2) - \delta_0).\end{aligned}$$

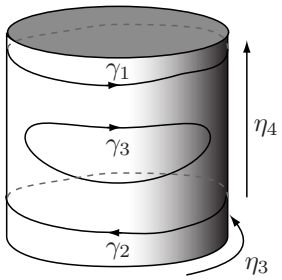

Fig. 3. Three phase curves illustrating Lemma 3.12. The high-energy curves γ_1 and γ_2 are homeomorphic to circles $\{\eta_4 = \text{constant}\}$, while the low-energy curve γ_3 is homeomorphic to a circle $\{(\eta_3 - \bar{\eta}_3)^2 + \eta_4^2 = \text{constant}\}$.

By the curvature bound in Assumption 1, $-(\mu/\epsilon) + \varphi'(\theta_0 + L/2) - \delta_0 < -\mu/\epsilon < 0$, implying that $V''(\theta_0 + L/2) < 0$, and so the equilibrium $(\theta_0 + L/2, 0)$ is always unstable. On the other hand, depending on the curvature at θ_0, the equilibrium in $(\theta_0, 0)$ may or may not be stable. If there are exactly two equilibria, then f has exactly two zeros at $\eta_3 = \theta_0 + L/2$ and $\eta_3 = \theta_0$. Using the properties that f is odd with respect to θ_0, that $f'(\theta_0) \neq 0$, and that $f'(\theta_0 + L/2) > 0$, we have $f'(\theta_0) < 0$, and so $V''(\theta_0) > 0$, proving that the equilibrium at $(\theta_0, 0)$ is stable. □

Remark 3.11. In the case that $\mathcal{C}$ is a circle of length L, there are two equilibria at $(\theta_0, 0) = ([-L/4]_L, 0)$ and $(\theta_0 + L/2, 0) = ([L/4]_L, 0)$. They correspond to the south and north poles of the circle. The south pole is stable, while the north pole is unstable, so if the PVTOL is initialized on the roll manifold near the south pole of the circle with slow speed, the aircraft oscillates back and forth around this point while maintaining a bounded roll angle.

Lemma 3.12. Let $\underline{\mathcal{H}} := \min_{\eta_3 \in S^1} V(\eta_3)$ and $\overline{\mathcal{H}} := \max_{\eta_3 \in S^1} V(\eta_3)$. Then, all phase curves of (21) in the set $\{(\eta_3, \eta_4) \in S^1 \times \mathbb{R} : \mathcal{H}(\eta_3, \eta_4) > \overline{\mathcal{H}}\}$ are homeomorphic to circles $\{(\eta_3, \eta_4) \in S^1 \times \mathbb{R} : \eta_4 = \text{constant}\}$. On the other hand, almost all phase curves in the set $\{(\eta_3, \eta_4) \in S^1 \times \mathbb{R} : \underline{\mathcal{H}} < \mathcal{H}(\eta_3, \eta_4) < \overline{\mathcal{H}}\}$ are homeomorphic to circles $\{(\eta_3, \eta_4) : (\eta_3 - \bar{\eta}_3)^2 + \eta_4^2 = \text{constant}\}$.

In words, almost all phase curves are closed; high-energy phase curves correspond to complete rotations of η_3 around S^1 in either direction, while low-energy ones correspond to oscillations around a point in S^1, see Figure 3.

Proof. Each phase curve of (21) lies entirely in a level set of $\mathcal{H}$. We have

$$\mathcal{H}^{-1}(h) = \{(\eta_3, \eta_4) : |\eta_4| = \sqrt{[2/M(\eta_3)](h - V(\eta_3))}\}. \tag{22}$$

If $h > \overline{\mathcal{H}}$, $\mathcal{H}^{-1}(h)$ is homeomorphic to two disjoint circles $\{\eta_4 = \pm 1\}$. The homeomorphism in question is $(\eta_3, \eta_4) \mapsto (\eta_3, \eta_4/\sqrt{[2/M(\eta_3)](h - V(\eta_3))}\}$. Since $|\eta_4| > 0$ on $\mathcal{H}^{-1}(h)$, it follows that there are no equilibria on this level set, and so the level set $\mathcal{H}^{-1}(h)$ is composed by exactly two disjoint phase curves with opposite orientation (in Figure 3, the curves γ_1 and γ_2).

Now suppose that $h \in (\underline{\mathcal{H}}, \overline{\mathcal{H}})$. Then, the set $\{\eta_3 : V(\eta_3) = h\}$ is non-empty. By Sard's theorem [8] the set of regular values of $V(\eta_3)$ (i.e., values $h \in \text{Im}(V)$ such that $V'(\eta_3) \neq 0$ for all $\eta_3 \in V^{-1}(h)$) has full measure in $\text{Im}(V)$. Therefore, for almost all h, $V' \neq 0$ on $V^{-1}(h)$. Assume that h is such a regular value of V. Then, the set $V^{-1}(h)$ is a zero-dimensional closed embedded submanifold of S^1. In other words, the set $V^{-1}(h)$ is given by a finite number (because S^1 is compact) of isolated points. In the proof of Lemma 3.9 we have shown that V' is odd, and so V is an even function. Therefore, the set $V^{-1}(h)$ has an even number of points, $2n$ of them ($n \geq 1$), dividing S^1 into $2n$ intervals. The sign of $h - V(\eta_3)$ is constant over each interval and alternates among any two adjacent intervals. In particular, there are n disjoint intervals on S^1 on which $h - V(\eta_3) \geq 0$, with equality holding only at the boundary of the intervals. Consider any one such interval $[\eta_3^1, \eta_3^2]$, with $V(\eta_3^1) = V(\eta_3^2) = h$, and $h - V(\eta_3) > 0$ on (η_3^1, η_3^2). Since $V' \neq 0$ on $V^{-1}(h)$, it must be that $V'(\eta_3^1) < 0$ and $V'(\eta_3^2) > 0$. In light of (22), the set $\mathcal{H}^{-1}(h)$ has n components. Each of them lies in a band $[\eta_3^1, \eta_3^2] \times \mathbb{R}$. Let $C = (\eta_3^1 + \eta_3^2)/2$ and $R = (\eta_3^2 - \eta_3^1)/2$ be the centre and radius of the interval, and consider the map $(\eta_3, \eta_4) \mapsto (\tilde{\eta}_3, \tilde{\eta}_4)$ defined as

$$(\eta_3, \eta_4) \mapsto \left(\eta_3, \eta_4 \sqrt{\frac{R^2 - (\eta_3 - C)^2}{\frac{2}{M(\eta_3)}(h - V(\eta_3))}}\right).$$

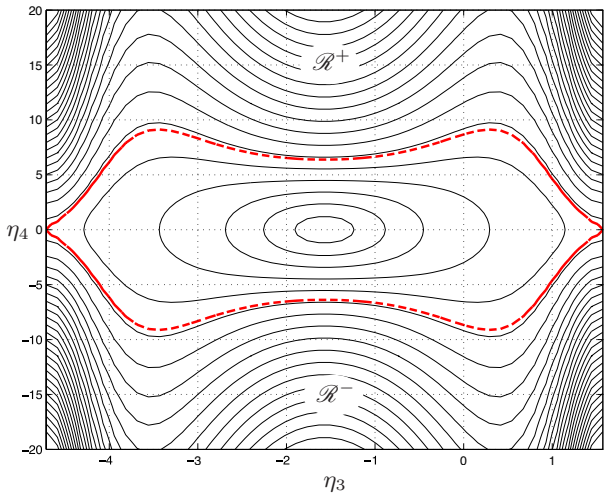

Fig. 4. Phase portrait of the (η_3, η_4)-dynamics on the roll dynamics manifold $\Gamma_2^\star$ in the case when the path to be followed is the unit circle. For convenience, the phase portrait is displayed on the plane, but actually the η_3 axis wraps around, so that the points on the lines $\eta_3 = \pi/2$ and $\eta_3 = -(3/2)\pi$ in the figure are identified.

The map above is a homeomorphism on $(\eta_3^1, \eta_3^2) \times \mathbb{R}$. Actually, it is a homeomorphism on $[\eta_3^1, \eta_3^2] \times \mathbb{R}$. To see this, it suffices to notice that $2/M(\eta_3)$ is always positive and the limits

$$\lim_{\eta_3 \to \eta_3^{1,2}} \frac{R^2 - (\eta_3 - C)^2}{h - V(\eta_3)} = \frac{-2(\eta_3^{1,2} - C)}{-V'(\eta_3^{1,2})}$$

are both positive numbers. The image of the component of $\mathcal{H}^{-1}(h)$ contained in $[\eta_3^1, \eta_3^2] \times \mathbb{R}$ is the circle $\{(\tilde{\eta}_3, \tilde{\eta}_4) : (\tilde{\eta}_3 - C)^2 + \tilde{\eta}_4^2 = R^2\}$. Since $V' \neq 0$ on $V^{-1}(h)$, there are no equilibria in $\mathcal{H}^{-1}(h)$, and so each component of $\mathcal{H}^{-1}(h)$ coincides with exactly one phase curve of (21) (in Figure 3, the curve γ_3). □

Remark 3.13. To better illustrate Lemma 3.12, consider the unit circle (length $L = 2\pi$) centred at the origin, and set $\mu = \epsilon = 1$. The level sets of $\mathcal{H}(\eta_3, \eta_4)$, forming the phase portrait of the motion on the roll dynamics manifold, are shown in Figure 4. The level set $\{\mathcal{H}(\eta_3, \eta_4) = \overline{\mathcal{H}}\}$ is displayed with a thick dashed line. If the PVTOL is initialized in the region enclosed by this curve, then the PVTOL oscillates on the circle around the south pole without completing the revolution on the circle. On the other hand, if the PVTOL is initialized in the region $\mathscr{R}^+$ (resp., $\mathscr{R}^-$), then the PVTOL traverses the entire circle in the counterclockwise (resp., clockwise) direction indefinitely and with bounded speed. All predictions of Lemma 3.12 are consistent with this phase portrait. Figure 4 also illustrates that the equilibrium $(\eta_3, \eta_4) = ([\pi/2]_{2\pi}, 0)$ is unstable, while the equilibrium $([-\pi/2]_{2\pi}, 0)$ is stable, as predicted by Lemma 3.10.

Corollary 3.14. Let $\mathscr{R}^+ = \{(\eta_3, \eta_4) \in S^1 \times \mathbb{R} : \mathcal{H}(\eta_3, \eta_4) > \overline{\mathcal{H}}, \eta_4 > 0\}$ and $\mathscr{R}^- = \{(\eta_3, \eta_4) \in S^1 \times \mathbb{R} : \mathcal{H}(\eta_3, \eta_4) > \overline{\mathcal{H}}, \eta_4 < 0\}$. Then, for any initial condition in $\mathscr{R}^+$ (resp., $\mathscr{R}^-$), the PVTOL traverses $\mathcal{C}$ in the positive (resp., negative) direction with angular velocity $|\eta_4(t)|$ bounded away from zero and bounded from above. Moreover, its roll angle $\eta_1(t) = f(\eta_3(t))$ is a periodic function with zero mean, implying that the aircraft does not undergo multiple revolutions about its longitudinal axis.

Proof. By Lemma 3.12, any initial condition in $\mathscr{R}^+$ ($\mathscr{R}^-$) gives rise to a closed orbit $(\eta_3(t), \eta_4(t))$ with $\eta_4(t) > 0$ ($\eta_4 < 0$) corresponding to a complete rotation around $\mathcal{C}$ in the positive (negative) direction. Since the orbit is closed, $|\eta_4(t)|$ is bounded from above. Recall (see property (ii) in Section 3.4) that $f(\eta_3)$ is an odd function. This fact, together with the property that $\eta_3(t)$ is a periodic signal with $\mathrm{Im}(\eta_3(t)) = S^1$, implies that $t \mapsto f(\eta_3(t))$ has zero mean. □

4 Main result

The overall controller designed in the previous section is

$$
\begin{aligned}
&\begin{bmatrix} u_1 \\ u_2 \end{bmatrix} = R^{-1}(x_5) D^{-1}(\mathrm{col}(x_1, x_3)) \\
&\qquad \left(- \begin{bmatrix} \dot{d\pi} \\ \dot{d\gamma} \end{bmatrix} \mathrm{col}(x_2, x_4) + g \begin{bmatrix} \partial_{x_3} \pi \\ \partial_{x_3} \gamma \end{bmatrix} + \begin{bmatrix} v^{\parallel} \\ v^{\pitchfork} \end{bmatrix} \right), \\
&v^{\pitchfork}(\xi) = -\frac{1}{k_1} \left(\mathrm{sgn}\,(k_1 \xi_2) |k_1 \xi_2|^{\frac{1}{2}} + \mathrm{sgn}\,(\phi(\xi)) |\phi(\xi)|^{\frac{1}{3}} \right), \\
&v^{\parallel}(\eta) = \frac{\beta(\eta_1, \eta_3, \eta_4) - w(e)}{f'(\eta_3) - \frac{\mu}{\epsilon} \cos(\eta_1 - \varphi(\eta_3))}, \\
&\phi(\xi) = k_1 \xi_1 + \frac{2}{3} \mathrm{sgn}\,(k_1 \xi_2) |k_1 \xi_2|^{\frac{3}{2}} \\
&\beta(\eta_1, \eta_3, \eta_4) = \frac{\mu}{\epsilon} (g \sin \eta_1 + [\sin(\eta_1 - \varphi(\eta_3)) \varphi'(\eta_3)) \\
&\qquad\qquad - f''(\eta_3)] \eta_4^2, \\
&w(e) = -\frac{1}{k_2} \Big(\mathrm{sgn}\,(k_2 e_2) |k_2 e_2|^{\frac{1}{2}} \\
&\qquad + k_2^{\frac{1}{3}} \mathrm{sgn}\,(\sin(\psi(e))) \, |\sin(\psi(e))|^{\frac{1}{3}} \Big), \\
&\psi(e) = e_1 + \frac{2}{3} k_2^{\frac{1}{2}} \mathrm{sgn}(e_2) \, |e_2|^{\frac{3}{2}}.
\end{aligned}
\tag{23}
$$

Theorem 4.1. The continuous feedback (23), where (η, ξ) are defined in (6), D is as in (5), $f(\eta_3)$ is as in (15) (with δ_0 as in (14), and K as in (16)), solves PFP.

We stress that our solution to PFP is local, in that the controller (23) is guaranteed to work in a neighborhood of $\Gamma_2^\star$. In particular, the PVTOL's centre of mass should be initialized in a neighborhood of $\mathcal{C}$.

Proof. The transversal controller meets goal **G1** and **G2**. Suppose we want to solve PFP by following $\mathcal{C}$ in the positive direction. We select an open set U of initial conditions as follows. Fix $\varepsilon_2 > \varepsilon_1 > 0$ and let $\mathscr{R}^+_{\varepsilon_1, \varepsilon_2}$ be the subset of points in $\mathscr{R}^+$ whose distance from the boundary of $\mathscr{R}^+$ is at least ε_1, but no more than ε_2. Fix $\zeta > 0$, and define the bounded sets $U^\eta := \{\eta : (\eta_3, \eta_4) \in \mathscr{R}^+_{\varepsilon_1, \varepsilon_2}, |e_1| = |\eta_1 - f(\eta_3)| < \zeta, |e_2| = |\eta_2 - f'(\eta_3)\eta_4| < \zeta\}$ and $U^\xi = \{\xi : \|\xi\| < \zeta\}$. Trajectories $\xi(t)$ of the transversal subsystem converge to zero in a finite time which is uniform over compact sets of initial conditions. Therefore, there exists $T_1 > 0$ such that all trajectories $\xi(t)$ with $\|\xi(0)\| < \zeta$ converge to zero in less than time T_1. If ζ is small, then T_1 is small and therefore $\eta(T_1) - \eta(0)$ is small. In particular, if $\eta(0)$ is in U^η, then $|e_1(T_1)|$ and $|e_2(T_1)|$ are slightly larger than ζ, but of order ζ. The tangential controller has the same finite-time convergence properties as the transversal one, so there exists a time $T_2 > T_1$ such that $e_1(T_2) = e_2(T_2) = 0$ for all $\eta(0) \in U^\eta$. If ζ is small, then so is T_2, and therefore $\|\eta(T_2) - \eta(0)\|$ is small of order ζ, for all $\eta(0) \in U^\eta$. Since $(\eta_3(0), \eta_4(0))$ is in the interior of $\mathscr{R}^+$, with distance at least ε_1 from the boundary, one can pick ζ small enough that $(\eta_3(T_2), \eta_4(T_2))$ is still in $\mathscr{R}^+$. Then, by Corollary 3.14, for all $t \geq T_2$, the PVTOL traverses $\mathcal{C}$ in the positive direction with bounded speed, and the roll angle $\eta_1(t)$ is a periodic function with zero mean. Therefore, goals **G3** and **G4** are met. In conclusion, the set U of initial conditions is defined as $T^{-1}(U^\eta \times U^\xi)$. If necessary, it can be made smaller so that $U \subset V$, the domain of definition of T. Note that $h(U)$ contains $\mathcal{C}$ because, in (η, ξ) coordinates, $h^{-1}(\mathcal{C}) = \{\xi_1 = 0\}$. □

5 Implementation issues and examples

In this section we discuss implementation details for the feedback controller (23) and present simulation results for two examples. The control law (23) requires the computation of the coordinate transformation $(x_1, \ldots, x_6) \mapsto (\eta_1, \ldots, \eta_4, \xi_1, \xi_2)$ defined in Equation (6). Since $\eta_1 = x_5$ and $\eta_2 = x_6$ in (6), only the computation of the states η_3, η_4, ξ_1, ξ_2 requires further explanation. The definition of these variables relies on

(i) a unit speed speed parametrization $\tilde{\sigma}(t)$ of $\mathcal{C}$,
(ii) an implicit representation of $\mathcal{C}$, $\mathcal{C} = \{y : \gamma(y) = 0\}$, and
(iii) the function $\pi : \mathbb{R}^2 \to S^1$ mapping a point (x_1, x_3) in a neighborhood of $\mathcal{C}$ to the arc length θ characterizing the closest point on $\mathcal{C}$.

In practice, it is often the case that a parametrization of $\mathcal{C}$ is available which does not have unit speed, and it may be impossible to find a unit speed parametrization in closed form. Additionally, while an implicit representation of a planar Jordan curve is guaranteed to exist, the curve may be provided in parametrized form. In the next two sections, we discuss how to compute η_3, η_4, ξ_1, and ξ_2 from $(x_1, \ldots, x_6)$ in the two cases when $\mathcal{C}$ is only given in parametrized form, but does not have unit speed, and when an implicit representation of $\mathcal{C}$ is available (but, again, the parametrization does not have unit speed).

5.1 Parameterized curves

Suppose the regular Jordan curve $\mathcal{C}$ of length L is given as the image of a smooth T-periodic parametrization $\hat{\sigma} = \operatorname{col}(\hat{\sigma}_1, \hat{\sigma}_2) : \mathbb{R} \longrightarrow \mathbb{R}^2$, which does not necessarily have unit speed (and hence $T \neq L$). We begin with the computation of $\eta_3 = \pi(x_1, x_3) = \arg\min_{\theta \in S^1} \| \operatorname{col}(x_1, x_3) - \sigma(\theta)\|$, where $\sigma(\theta)$ is the unknown unit speed parametrization of $\mathcal{C}$.

(a) Numerically calculate

$$t^\star = \hat{\pi}(x_1, x_3) := \left[\arg \min_{t \in [0,T]} \| \operatorname{col}(x_1, x_3) - \hat{\sigma}(t)\| \right]_T . \tag{24}$$

where $T > 0$ is the period of $\hat{\sigma}$. Analogously to the function π defined in Section 3.2, the function $\hat{\pi} : \mathbb{R}^2 \to [0, T]$ is well-defined in a tubular neighbourhood $\mathcal{C}^\varepsilon$ of $\mathcal{C}$. The calculation in (24) is a line search problem which can be effectively implemented because the derivative of $\| \operatorname{col}(x_1, x_3) - \hat{\sigma}(t)\|$ with respect to t is available in closed form.

(b) Numerically compute the integral

$$g(t) := \int_0^t \|\hat{\sigma}'(\tau)\| d\tau. \tag{25}$$

(c) The state $\eta_3 = \pi(x_1, x_3)$ can now be computed as $\eta_3 = g \circ \hat{\pi}(x_1, x_3) = g(t^\star)$.

Next, we turn to the computation of ξ_1. Computing ξ_1 amounts to finding an implicit representation of $\mathcal{C}$, $\mathcal{C} = \{\gamma(y) = 0\}$, from the parametrization $\hat{\sigma}$. For any $\eta_3 \in S^1$, define $\tau(\eta_3) := R_{\frac{\pi}{2}} \sigma'(\eta_3)$, where $R_{\frac{\pi}{2}}$ is the counter-clockwise rotation by $\pi/2$. This way, $\tau(\eta_3)$ represents the unit normal vector to $\mathcal{C}$ at the point $\sigma(\eta_3)$, and $\{\sigma'(\eta_3), \tau(\eta_3)\}$ is the Frenet-Serret frame for $\mathcal{C}$. Let $y = \operatorname{col}(x_1, x_3)$; since the vector $y - \sigma(\eta_3)$ is parallel to $\tau(\eta_3)$, we can write

$$\begin{aligned} y &= \sigma(\eta_3) + \tau(\eta_3)\xi_1 \\ &= \sigma(\pi(y)) + \tau(\pi(y))\xi_1. \end{aligned} \tag{26}$$

Solving the above equation for ξ_1, we get an implicit representation of $\mathcal{C}$:

$$\begin{aligned} \xi_1 &= \langle \tau(\pi(y)),\ y - \sigma(\pi(y)) \rangle \\ &= \left\langle R_{\frac{\pi}{2}} \frac{\hat{\sigma}'(t^\star)}{\|\hat{\sigma}'(t^\star)\|},\ y - \hat{\sigma}(t^\star) \right\rangle \Bigg|_{t^\star = \hat{\pi}(y)} \\ &= \frac{1}{\|\hat{\sigma}'(t^\star)\|} \left\langle R_{\frac{\pi}{2}} \hat{\sigma}'(t^\star),\ y - \hat{\sigma}(t^\star) \right\rangle \big|_{t^\star = \hat{\pi}(y)} =: \gamma(y). \end{aligned}$$

The expression above follows from the fact that $\sigma'(\pi(y)) = \hat{\sigma}'(\hat{\pi}(y))/\|\hat{\sigma}'(\hat{\pi}(y))\|$ and that $\sigma \circ \pi = \hat{\sigma} \circ \hat{\pi}$. To calculate ξ_2 and η_4, we take derivatives of (26)

$$\begin{aligned} \dot{y} &= \sigma'(\pi(y)) \langle d\pi_y,\ \dot{y} \rangle + \tau'(\pi(y)) \langle d\pi_y,\ \dot{y} \rangle \xi_1 + \tau(\pi(y))\dot{\xi}_1 \\ &= \sigma'(\pi(y))\eta_4 + \tau'(\pi(y))\eta_4\xi_1 + \tau(\pi(y))\xi_2, \end{aligned}$$

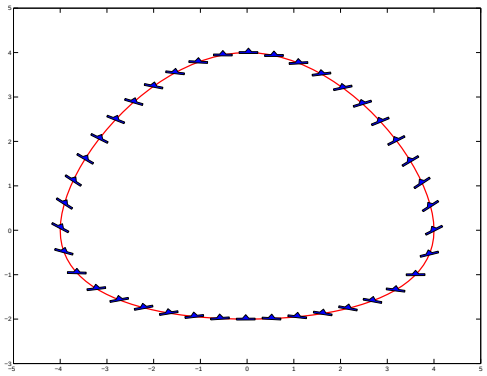

(a) The curve $\mathcal{C}$ and the configuration of the PVOTL on the roll dynamics manifold. Notice the symmetry of the configuration with respect to the vertical axis passing through the centre of the curve.

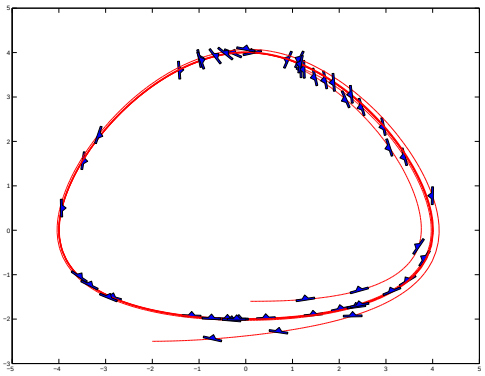

(b) Simulation results of the path following controller using the numerical procedures presented in Section 5.1.

Fig. 5. Path following for the cubic spline example in Section 5.1.

and note that $\tau'(\pi(y)) = -\varphi'(\pi(y))\sigma'(\pi(y))$ where $\varphi'(\pi(y))$ is the signed curvature of $\mathcal{C}$ at $\sigma(\pi(y))$. It then follows that

$$\dot{y} = \sigma'(\pi(y))\,(1 - \varphi'(\pi(y))\xi_1)\,\eta_4 + \tau(\pi(y))\xi_2.$$

The equation above can be solved for (η_4, ξ_2) on the neighborhood of $\mathcal{C}$, $\{y \in \mathbb{R}^2 : |1 - \varphi'(\pi(y))\xi_1| > 0\}$,

$$\begin{aligned} \eta_4 &= \frac{1}{(1 - \varphi'(\pi(y))\xi_1)}\,\langle \sigma'(\pi(y)),\ \dot{y}\rangle \\ \xi_2 &= \langle \tau(\pi(y)),\ \dot{y}\rangle\,. \end{aligned} \tag{27}$$

In conclusion, η_4 and ξ_2 are calculated as follows

$$\begin{aligned} \varphi'(\pi(x_1, x_3)) &= \left.\frac{\hat{\sigma}_1'(t^\star)\hat{\sigma}_2''(t^\star) - \hat{\sigma}_1''(t^\star)\hat{\sigma}_1'(t^\star)}{\|\hat{\sigma}'(t^\star)\|^3}\right|_{t^\star = \hat{\pi}(x_1, x_3)} \\ \eta_4 &= \left.\frac{1}{(1 - \varphi'(\pi(x_1, x_3))\xi_1)}\,\frac{(\hat{\sigma}'(t^\star))^\top}{\|\hat{\sigma}'(t^\star)\|}\begin{bmatrix} x_2 \\ x_4 \end{bmatrix}\right|_{t^\star = \hat{\pi}(x_1, x_3)} \\ \xi_2 &= \left.\frac{(\hat{\sigma}'(t^\star))^\top}{\|\hat{\sigma}'(t^\star)\|}\begin{bmatrix} x_4 \\ -x_2 \end{bmatrix}\right|_{t^\star = \hat{\pi}(x_1, x_3)}. \end{aligned}$$

As an example, consider the case in which $\hat{\sigma}$ is a cubic spline (a C^2 function defined piecewise by cubic polynomials). Splines allow one to define regular curves passing though a set of assigned points in $\mathbb{R}^2$ and are a useful tool for trajectory planning. In this example, we set $\mu/\epsilon = 1$. Figure 5(a) represents the periodic cubic spline passing trough points $y_1 = \mathrm{col}\,(4, 0)$, $y_2 = \mathrm{col}\,(0, 4)$, $y_3 = \mathrm{col}\,(-4, 0)$, $y_4 = \mathrm{col}\,(0, -2)$. This spline has a vertical symmetry axis passing through the origin, therefore part (i) of Assumption 1 is satisfied. Moreover, its length is $L = 22.06$ and its maximum curvature is less than 0.75, so part (ii) is also satisfied. Figure 5(a) also illustrates the configuration of the PVTOL on the roll dynamics manifold, while Figure 5(b) shows some PVTOL trajectories obtained with our path following controller.

5.2 Implicitly represented curves

When the curve $\mathcal{C}$ is given in implicit form, $\mathcal{C} = \{y : \gamma(y) = 0\}$, with $\|d\gamma_y\|$ not necessarily unit length for $y \in \mathcal{C}$, the calculations of the transversal states ξ_1 and ξ_2 are simplified. However, in such cases a smooth parameterization of

$\mathcal{C}$ is still needed in order to compute the tangential states η_3, η_4. Suppose that $\mathcal{C}$ has a sufficiently smooth (at least C^3) parametric representation [2], i.e., $\mathcal{C} = \mathrm{Im}\,(\hat{\sigma})$ where $\hat{\sigma} : \mathbb{R} \to \mathbb{R}^2$ is not necessarily a unit speed parametrization. The transversal states can be computed directly with the help of symbolic algebra software to obtain

$$\begin{aligned}\xi_1 &= \frac{\gamma(x_1, x_3)}{\|d\gamma_{(x_1,x_3)}\|} \\ \xi_2 &= \left[\begin{array}{cc} \partial_{x_1} \frac{\gamma(x_1,x_3)}{\|d\gamma_{(x_1,x_3)}\|} & \partial_{x_3} \frac{\gamma(x_1,x_3)}{\|d\gamma_{(x_1,x_3)}\|} \end{array}\right] \mathrm{col}\,(x_2, x_4)\end{aligned}$$

The calculation of η_3 can be done as presented in Section 5.1: $\eta_3 = g \circ \hat{\pi}(x_1, x_3)$. For η_4, we use the following calculations

$$\begin{aligned}\eta_4 &= d\pi_{(x_1,x_3)} \begin{bmatrix} x_2 \\ x_4 \end{bmatrix} \\ &= \left.\frac{dg}{dt}\right|_{\hat{\pi}(x_1,x_3)} d\hat{\pi}_{(x_1,x_3)} \begin{bmatrix} x_2 \\ x_4 \end{bmatrix} \\ &= \|\hat{\sigma}'(\hat{\pi}(x_1, x_3))\| d\hat{\pi}_{(x_1,x_3)} \begin{bmatrix} x_2 \\ x_4 \end{bmatrix}.\end{aligned}$$

Next, we need to find an expression for $d\hat{\pi}$. First, we note that, using arguments completely analogous to those in the proof of Lemma 3.2, $\left(d\hat{\pi}_{(x_1,x_3)}\right)^\top = k(x_1, x_3)\hat{\sigma}'(\hat{\pi}(x_1, x_3))$ where $k : \mathcal{C}^\varepsilon \to \mathbb{R}$ is a smooth scalar function. To find $k(x_1, x_3)$, we differentiate the identity $\hat{\pi}(x_1, x_3) = \hat{\pi}\left(\hat{\sigma}\left(\hat{\pi}(x_1, x_3)\right)\right)$ to get

$$d\hat{\pi}_{(x_1,x_3)} = d\hat{\pi}_{\hat{\sigma}\circ\hat{\pi}(x_1,x_3)}\hat{\sigma}'(\hat{\pi}(x_1, x_3))d\hat{\pi}_{(x_1,x_3)},$$

which implies $d\hat{\pi}_{\hat{\sigma}\circ\hat{\pi}(x_1,x_3)}\hat{\sigma}'(\hat{\pi}(x_1, x_3)) = 1$, or

$$k(x_1, x_3)\left(\hat{\sigma}'(\hat{\pi}(x_1, x_3))\right)^\top \hat{\sigma}'(\hat{\pi}(x_1, x_3)) = 1,$$

and therefore $k(x_1, x_3) = 1/\|\hat{\sigma}'(\hat{\pi}(x_1, x_3))\|^2$. Hence, $d\hat{\pi}_{(x_1,x_3)} = \left(\hat{\sigma}'(\hat{\pi}(x_1, x_3))\right)^\top / \|\hat{\sigma}'(\hat{\pi}(x_1, x_3))\|^2$ and so

$$\eta_4 = \frac{\left(\hat{\sigma}'(\hat{\pi}(x_1, x_3))\right)^\top}{\|\hat{\sigma}'(\hat{\pi}(x_1, x_3))\|} \begin{bmatrix} x_2 \\ x_4 \end{bmatrix}.$$

To illustrate the required calculations, consider Cassini's oval [11]. The Cartesian equation of this curve is $\mathcal{C} := \{(x_1, x_3) \in \mathbb{R}^2 : \gamma(x_1, x_3) = \left(x_1^2 + x_3^2 + a^2\right)^2 - 4a^2x_1^2 - b^4 = 0\}$. The curve is illustrated in Figure 6(a) for $a = 3$ and $b = 1.05a$. The curve $\mathcal{C}$ has a smooth parametric representation where $\hat{\sigma} : \mathbb{R} \to \mathbb{R}^2$ is given by

$$\begin{aligned}\hat{\sigma}(t) &:= \begin{bmatrix} R(t)\cos(t) \\ R(t)\sin(t) \end{bmatrix} \\ R(t) &:= \sqrt{a^2\cos(2t) + \sqrt{b^4 - \left(a^2\sin(2t)\right)^2}}.\end{aligned} \tag{28}$$

It is easy to check that the curve (28) is regular, has length $L = 21.518$ and period $T = 2\pi$. Based on Figure 6(a) it is clear that there is a vertical axis of symmetry corresponding to the x_3 axis and hence part (i) of Assumption 1 is satisfied with $\theta_0 = [-L/4]_L = 3L/4 = 16.1385$. Figure 6(b) shows that when $\mu/\epsilon = 1$, part (ii) of Assumption 1 is also satisfied. Figure 7 shows the PVTOL trajectories obtained from the path following controller.

[2] If $\mathcal{C}$ is connected then there is a regular parameterized curve $\hat{\sigma}$ whose image is the whole of $\mathcal{C}$ [22].

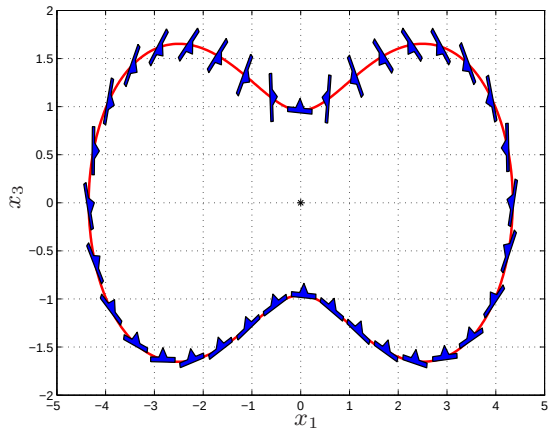

(a) The desired path for the PVTOL's centre of mass, a Cassini oval with $a = 3$ and $b = 1.05a$. The figure also illustrates the configuration of the PVTOL on the roll dynamics manifold.

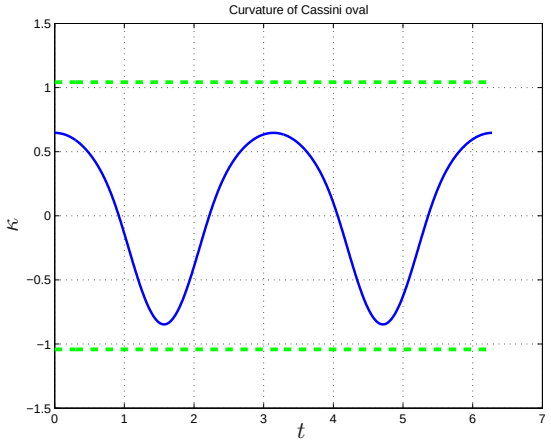

(b) The curvature of the Cassini oval with $a = 3$ and $b = 1.05a$. The dashed line represents the maximum allowable curvature when $\mu/\epsilon = 1$.

Fig. 6. Path to be followed in Section 5.2.

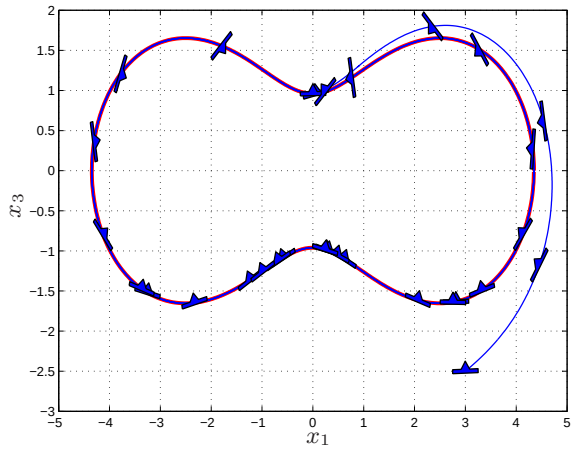

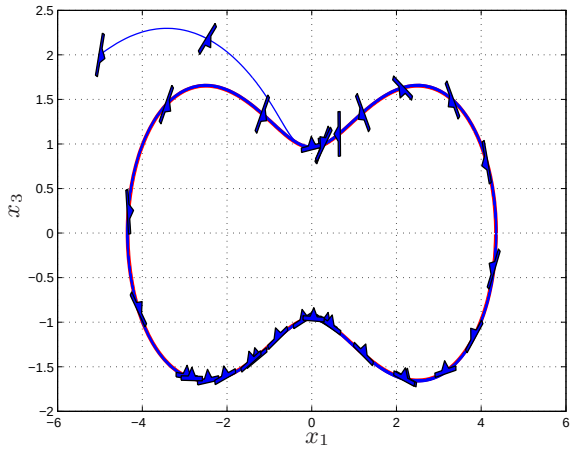

Fig. 7. Simulation results of the path following controller and Cassini's oval.

Acknowledgements

L. Consolini and M. Tosques were partially supported by MIUR scientific funds in the framework of a PRIN project. M. Maggiore and C. Nielsen were supported by the National Science and Engineering Research Council (NSERC) of Canada.

References

[1] S.A. Al-Hiddabi and N.H. McClamroch. Tracking and maneuver regulation control for nonlinear non-minimum phase systems: Application to flight control. *IEEE Transactions on Control Systems Technology*, 10(6):780–792, November 2002.

[2] S.P. Bhat and D.S. Bernstein. Continuous finite-time stabilization of the translational and rotational double integrators. *IEEE Transactions on Automatic Control*, 43(5):678–682, 1998.

[3] S.P. Bhat and D.S. Bernstein. Finite-time stability of continuous autonomous systems. *SIAM Journal of Control and Optimization*, 38(3):751–766, 2000.

[4] L. Consolini and M. Tosques. On the VTOL exact tracking with bounded internal dynamics via a Poincaré map approach. *IEEE Transactions on Automatic Control*, 52(9):1757–1762, 2007.

[5] K.D. Do, Z.P. Jiang, and J. Pan. On global tracking control of a VTOL aircraft without velocity measurements. *IEEE Transactions on Automatic Control*, 48(12):2212–2217, December 2003.

[6] L. Freidovich, A. Robertsson, A. Shiriaev, and R. Johansson. Periodic motions of the pendubot via virtual holonomic constraints: Theory and experiments. *Automatica*, 44:785–791, 2008.

[7] F. Grognard and C. Canudas de Wit. Design of orbitally stable zero dynamics for a class of nonlinear systems. *Systems and Control Letters*, 51(2):89–103, 2004.

[8] V. Guillemin and A. Pollack. *Differential Topology.* Prentice Hall, New Jersey, 1974.

[9] J. Hauser and R. Hindman. Maneuver regulation from trajectory tracking: Feedback linearizable systems. In *Proceedings of the IFAC symposium on Nonlinear Control Systems Design*, pages 595 – 600, Tahoe City, CA, USA, June 1995.

[10] J. Hauser, S. Sastry, and G. Meyer. Nonlinear control design for slightly non-minimum phase systems: Applications to V/STOL aircraft. *Automatica*, 28(4):665–679, 1992.

[11] J. D. Lawrence. *A Catalog of Special Plane Curves.* Dover Publications, New York, 1972.

[12] F. Lin, W. Zhang, and R.D. Brandt. Robust hovering control of a PVTOL aircraft. *IEEE Transactions on Control Systems Technology*, 7(3):343–351, May 1999.

[13] L. Marconi, A. Isidori, and A. Serrani. Autonomous vertical landing on an oscillating platform: an internal-model based approach. *Automatica*, 38:21–32, 2002.

[14] P. Martin, S. Devasia, and B. Paden. A different look at output tracking: Control of a VTOL aircraft. In *IEEE Conference on Decision and Control*, pages 2376–2381, Lake Buena Vista, FL, USA, December 1994.

[15] P. Martin, S. Devasia, and B. Paden. A different look at output tracking: Control of a VTOL aircraft. *Automatica*, 32(1):101–107, 1996.

[16] C. Nielsen. *Set Stabilization Using Transverse Feedback Linearization.* PhD thesis, Dept. of Electrical and Computer Engineering, Univ. of Toronto, 2008.

[17] C. Nielsen, C. Fulford, and M. Maggiore. Path following using transverse feedback linearization: Application to a maglev positioning system. *Automatica*, 2009. Accepted.

[18] C. Nielsen and M. Maggiore. On local transverse feedback linearization. *SIAM J. Control and Optimization*, 47(5):2227–2250, 2008.

[19] G. Notarstefano, J. Hauser, and R. Frezza. Trajectory manifold exploration for the PVTOL aircraft. In *IEEE Conference on Decision and Control and European Control Conference*, pages 5848–5853, Seville, Spain, December 2005.

[20] R. Olfati-Saber. Global configuration stabilization for the VTOL aircraft with strong input coupling. *IEEE Transactions on Automatic Control*, 47(11):1949–1952, November 2002.

[21] F. Plestan, J.W. Grizzle, E.R. Westervelt, and G. Abba. Stable walking of a 7-DOF biped robot. *IEEE Transactions on Robotics and Automation*, 19(4):653–668, 2003.

[22] A. Pressley. *Elementary Differential Geometry.* Springer, New York, 2000.

[23] M. Saeki and Y. Sakaue. Flight control design for nonlinear non-minimum phase VTOL aircraft via two-step linearization. In *IEEE Conf. on Decision and Control*, pages 217–222, Orlando, FLA, USA, December 2001.

[24] A. Sanchez, P. Garcia, P. Castillo, and R. Lozano. Simple real-time stabilization of vertical takeoff and landing aircraft with bounded signals. *Journal of Guidance, Control, and Dynamics*, 31(4):1166–1175, 2008.

[25] A. Shiriaev, J.W. Perram, and C. Canudas de Wit. Constructive tool for orbital stabilization of underactuated nonlinear systems: Virtual constraints approach. *IEEE Transactions on Automatic Control.*, 50(8):1164–1176, August 2005.

[26] R. Wood and B. Cazzolato. An alternative nonlinear control law for the global stabilization of the PVTOL vehicle. *IEEE Transactions on Automatic Control*, 52(7):1282–1287, July 2007.

[27] A. Zavala-Río, I. Fantoni, and R. Lozano. Global stabilization of a PVTOL aircraft model with bounded inputs. *Intl. Journal of Control*, 76(18):1833–1844, 2003.